MULTI-COMPONENT FORCE BALANCE CONTROL SYSTEM

FINAL REPORT

on

NASA Grant NGR 47-005-026

Submitted by Co-Principal Investigators:

Dr. James W. Moore

Dr. Eugene S. McVey

and

Karl C. Henderson

Research Laboratories for the Engineering Sciences

University of Virginia

Charlottesville

Report No. EME-4029-103C-66U

August 1966

MULTI-COMPONENT FORCE BALANCE CONTROL SYSTEM

FINAL REPORT

on

NASA Grant NGR 47-005-026

Submitted by Co-Principal Investigators:

Dr. James W. Moore

Dr. Eugene S. McVey

and

Karl C. Henderson

RESEARCH LABORATORIES FOR THE ENGINEERING SCIENCES

SCHOOL OF ENGINEERING AND APPLIED SCIENCE

UNIVERSITY OF VIRGINIA

CHARLOTTESVILLE, VIRGINIA

Report No. EME-4029-103C-66U

August 1966

Copy No. 3

ABSTRACT

A new wind tunnel force measurement technique was necessitated by the introduction of hypersonic wind tunnels and small, heavy test models. A new technique is presented which uses a gas bearing to support the model and a control system which comprises three separate control loops to position the model. The three forces of interest - drag, lift, and pitch - are determined by sensing the servo motor currents and combining in a way to give the desired reading.

The servo loops are composed of sensors, amplifiers, and motors; each of which is described in detail. The theory for the design of the motors is presented.

The compensation of the servo loops is described wherein the open-loop data is obtained with the system running closed-loop.

A readout preparation unit is described which senses the currents and performs the appropriate addition and subtraction.

TABLE OF CONTENTS

LIST OF FIGURES

LIST OF SYMBOLS

a	coil radius for single turn approximation
e_m	servo motor input voltage
e_s	sensor output voltage
e_o	output voltage from compensation network
e_1	steady-state servo positioning voltage
e_2	input voltage to compensation network
i_{ss}	steady-state motor current
s	Laplace transform variable
x	displacement variable
x	rectangular coordinate
y	rectangular coordinate
z	rectangular coordinate
z	axial coordinate in cylindrical coordinate system
z_o	distance of single turn gradient coil from origin
$\hat{z}$	unit vector
B	magnetic field of gradient coil
F	aerodynamic force input
F	force on magnetic material
F_m	force exerted by servo motors
J_A	gradient coil current density
K	servo amplifier gain constant
K_b	constant of viscous friction

K_f	motor force constant
K_s	sensor constant
K_v	motor back emf constant
M	mass of supported portion of system
M	magnetic moment of permanent magnet
M_o	magnitude of magnetic moment of permanent magnet
V	permanent magnet volume
$\hat{V}_1, \hat{V}_2$	unit vectors in directions of axes of symmetry of gradient coils
∇	vector differential operator
β	angle between axes of symmetry of gradient coils
θ	angle between magnetic moment and axis of symmetry of gradient coils
μ_o	permeability of vacuum
ρ	radial coordinate
$\hat{\rho}$	unit vector in direction of radial coordinate
ω_n	system resonant frequency (open loop)

CHAPTER I

INTRODUCTION

GENERAL

A system is described in this thesis which is used to measure the forces on wind tunnel models. There are many other possible applications for this technique such as ion engine thrust measurement. Analytical and experimental work through the prototype stage has been completed, and actual wind tunnel operation should take place soon. The prototype is an operational system that can be effectively used in wind tunnels to measure lift, drag, and pitch force magnitudes from 0.005 pound to 0.5 pound in two ranges.

The development (1) of a new measurement technique was necessitated by wind tunnel model changes for hypersonic testing. At hypersonic velocities, wind tunnel models are relatively heavy and small because the models must be made of heat resistant materials and because of size limitations imposed on the tunnels. The ratio of model weight to aerodynamic force is the primary factor which necessitated the development of a new force measurement method. A typical range for the values of the ratio of model weight to aerodynamic force is 100:1 to 1:1. For ion engines this ratio may be one or two orders of magnitude more. An accuracy of 1% or better of full scale is desired.

Obviously, any system that must operate under these conditions should provide for the support of the model weight in such a way that the data does not need to be recovered from a reading that includes the model weight. In addition, the friction in the supports of existing systems would be a problem if they were used for this type application. The system that is to be described supports the model so that the steady-state data is independent of the model weight.

SYSTEM GENERAL DESCRIPTION

The balance system is shown schematically from the top in Fig. (1-1). The control loop for one of the y-direction servos and the readout equipment have been omitted for clarity. Briefly, the system operates in the following manner: the aerodynamic force displaces the model in the direction of the force. This displacement is sensed by the displacement sensor. The sensor output is amplified by the power amplifiers and applied to the servo motors. These motors drive the displacement toward zero. The motor current, being proportional to the force, is measured and calibration applied for the force reading.

The system may be divided into three main parts according to function:

1. Gas Bearing - The gas bearing serves two purposes. The first is the support of the model weight, and the second is to provide a practically frictionless

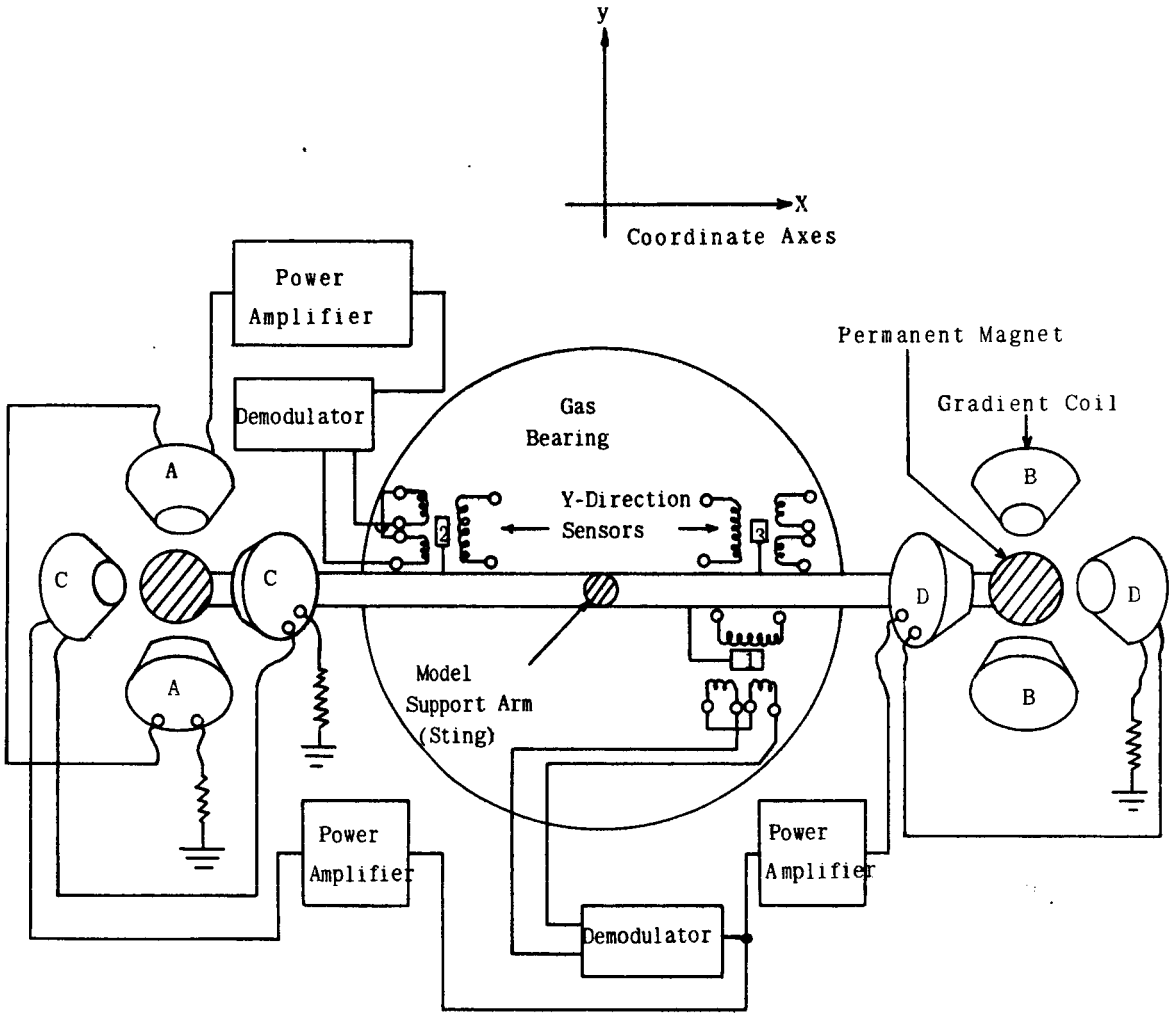

Figure 1-1

Schematic of Balance Servos

platform so that small steady-state motions are effected only by aerodynamic forces and the restoring forces of the control system. The analysis, design, and operation of this part of the system has been fully covered elsewhere (2, 3) and will not be considered here.

2. Control System - The control system is the primary subject of concern here. The purpose of the control system is the accurate positioning of the model in the plane of the forces. A complete description will be given later.
3. Readout Equipment - The readout equipment senses the motor currents required to null the control system and processes these measurements to provide readings of the three forces (4, 5) of interest--lift, drag, and pitch. This will also be fully described later.

The operation of the balance system can be explained in detail by considering each of the three desired forces separately, keeping in mind that the gas bearing is constrained in the xy-plane only by the servos. If a force is applied in the x-direction, the displacement is detected by sensor 1 which produces a voltage that is proportional to displacement. This voltage is applied to the two power amplifiers which are essentially voltage controlled current sources. The current through the gradient coils produces a force on the

permanent magnets which drives the displacement toward zero. Since the motor force is proportional to the current through the gradient coils, the aerodynamic force on the model can be determined by measuring the current through the motors and applying suitable calibration.

The operation of the system when a force is applied in the y-direction is essentially the same as in the x-direction except that there are two separate servos. Each y-direction servo responds to a force in the y-direction, and the force exerted by each is theoretically the same, i.e. each servo is required to balance half the applied force. The aerodynamic force in this direction is determined by measuring the current in each motor separately, summing, and applying suitable calibration.

The third aerodynamic force that must be measured is pitch. This is, in reality, a torque exerted in the xy-plane. If a torque is applied, one y-direction sensor will detect displacement in the positive y-direction while the other will detect a displacement in the negative y-direction. Thus, the y-direction motors will be exerting forces with opposite senses to accommodate the torque component. The magnitude of the torque is determined by measuring the motor currents, subtracting, and applying suitable calibration. The sense of the torque is obtained by noting the sign of the difference.

It can be seen from this discussion that an easily

measured quantity, current, is used to obtain the desired force readings. Furthermore, the sense of the force is indicated by the polarity of the reading. These two facts make readout instrumentation relatively simple.

It should be stated at this point that the direction of air (or plasma) flow through the tunnel is in the x-direction. The gas bearing, motors, and sensors are mounted outside the tunnel in the top. The test model is attached inside the tunnel to the model support arm (sting) which is, in turn, attached to the gas bearing. In order to measure lift and pitch in the chosen xy-plane, the model is rotated 90 degrees about the fore and aft axis. In other words, considering a model of a conventional winged aircraft, the wings are vertical rather than horizontal. In this way lift is a force toward one side of the tunnel and pitch is a torque in the xy-plane. With this configuration of model, motors, and sensors, the model weight is in the z-direction. Thus, the objective of making the steady-state data independent of the model weight is accomplished. Figure (1-2) is a schematic of the side view showing the gas bearing, model, and model support arm.

To this point the major emphasis has been on making the measurements independent of the model weight, but another factor that makes data reduction difficult is the effect that a force in one direction has on the reading of other forces being measured. This effect is call cross-coupling, and its

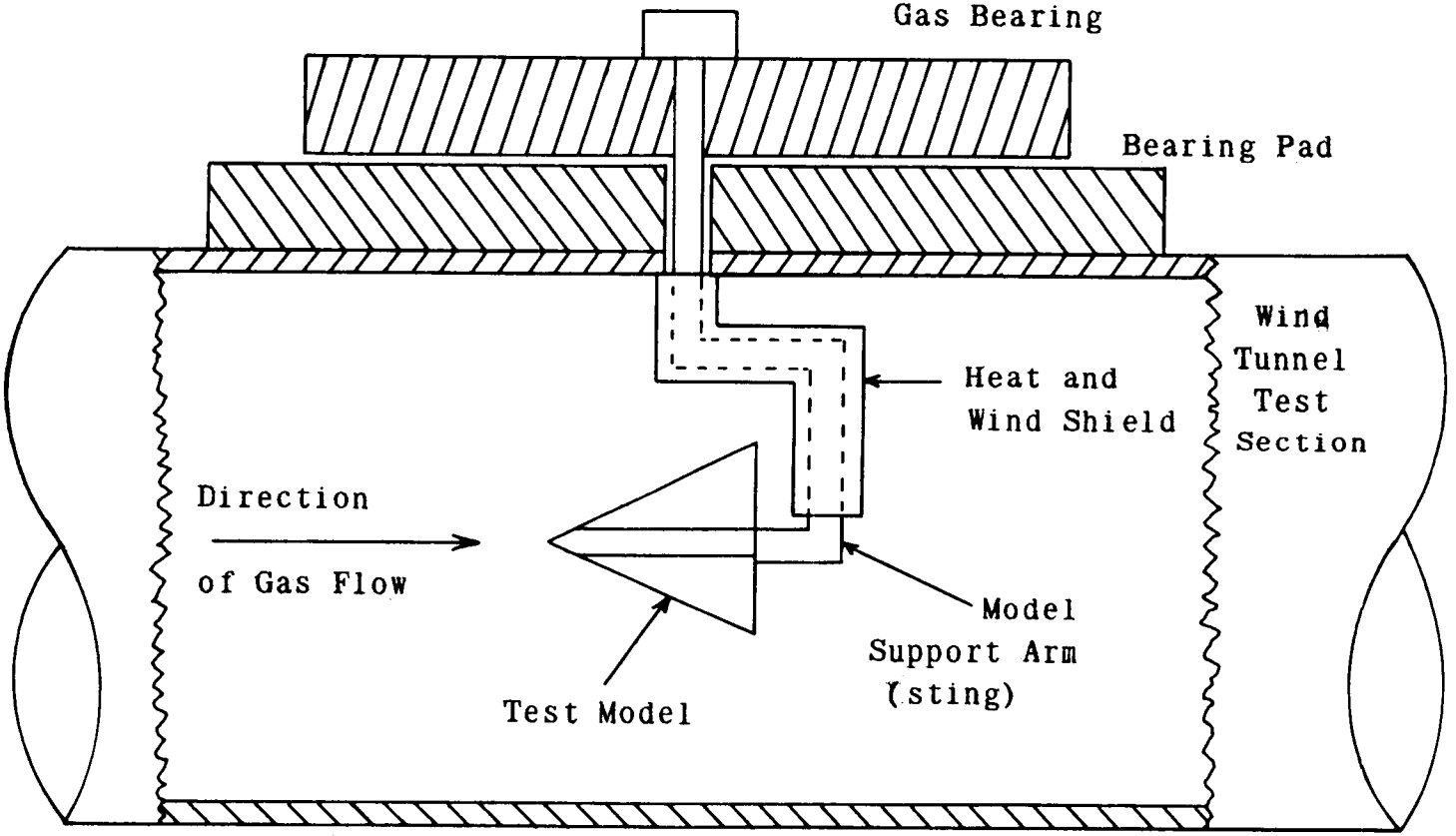

Figure 1-2

Schematic of Wind Tunnel Test Section

minimization is one of the primary considerations in the design of the system. The minimization of cross-coupling will be considered in Chapters III and IV.

CHAPTER II

SYSTEM ANALYSIS

ANALYSIS ASSUMING NO VISCOUS FRICTION

The development of the transfer function and block diagram for the system, disregarding viscous friction in the gas bearing, follows that given by Moore and McVey (1). This simplified analysis is presented because it will aid in understanding the design of this type of system. The analysis is also useful for obtaining information about the steady-state conditions of the system.

For the purposes of this development, the servos for lift and drag (y and x-directions respectively) will be considered independent of each other. The validity of this assumption has been verified by Mason (4, 5) where it is shown that the interaction of the servos (cross-coupling) is of the order of only 1%. The same analysis will apply theoretically to both directions. Only the x-direction servo will be considered.

The force balance equation for the x-direction is

$$F + F_m = M\ddot{x} \qquad (2\text{-}1)$$

where F is the aerodynamic force on the model (drag in this case), F_m is the force exerted by the servo motors, and M is the combined mass of the model, sting , gas bearing, and motor arm (i.e. the mass supported by the gas bearing).

The force exerted by the servo motors is proportional to the current, so

$$F_m = K_f i \tag{2-2}$$

where K_f is the constant of proportionality relating current to force.

Taking the Laplace transform of Eqs. (2-1) and (2-2), assuming zero initial conditions, and combining the results yields

$$F(s) + K_f i(s) = s^2 M x(s) \tag{2-3}$$

where s is the Laplace transform variable.

The motor inductance and servo amplifier output impedance will be assumed negligible in this first simplified analysis. This assumption will, of course, have to be verified for the motors and amplifiers that are used. With these assumptions, the relationship between the input voltage to the motor and the motor current is

$$e_m = iR + K_v \dot{x} \tag{2-4}$$

where K_v is the back emf constant of the motor, and R is the resistance of the motor winding. Taking the Laplace transform of Eq. (2-4) (again assuming zero initial conditions), and solving for the motor current yields

$$i(s) = \frac{e_m(s) - sK_v x(s)}{R} \tag{2-5}$$

The time constants of the servo amplifier can easily be made much smaller than the time constants of the mechanical part of the system so they can be ignored. Therefore the motor input voltage, e_m, is the servo error voltage times the gain constant, K, of the servo amplifier.

Assuming zero input voltage (any input voltage would simply be a dc positioning voltage), the servo error signal is the sensor output signal. Thus

$$e_m = K\, e_s(s) \tag{2-6}$$

where the phase reversal is introduced to produce negative feedback.

The final element in the loop is the position sensor. Any one of several types that are commercially available can be used if the largest time constant of the sensor chosen is much smaller than the significant time constants of the mechanical part of the system. Because the time constants of the sensor are not considered significant, the relation between sensor output and position is

$$e_s(s) = K_s x(s) \tag{2-7}$$

where K_s is the sensor constant.

The block diagram of Fig. (2-1) can now be drawn. This is the block diagram for the system in which the viscous friction of the gas bearing has been assumed negligible. As previously stated, the input voltage, e_1, is simply a dc positioning voltage and does not enter into any of the following calculations except the calculation of the

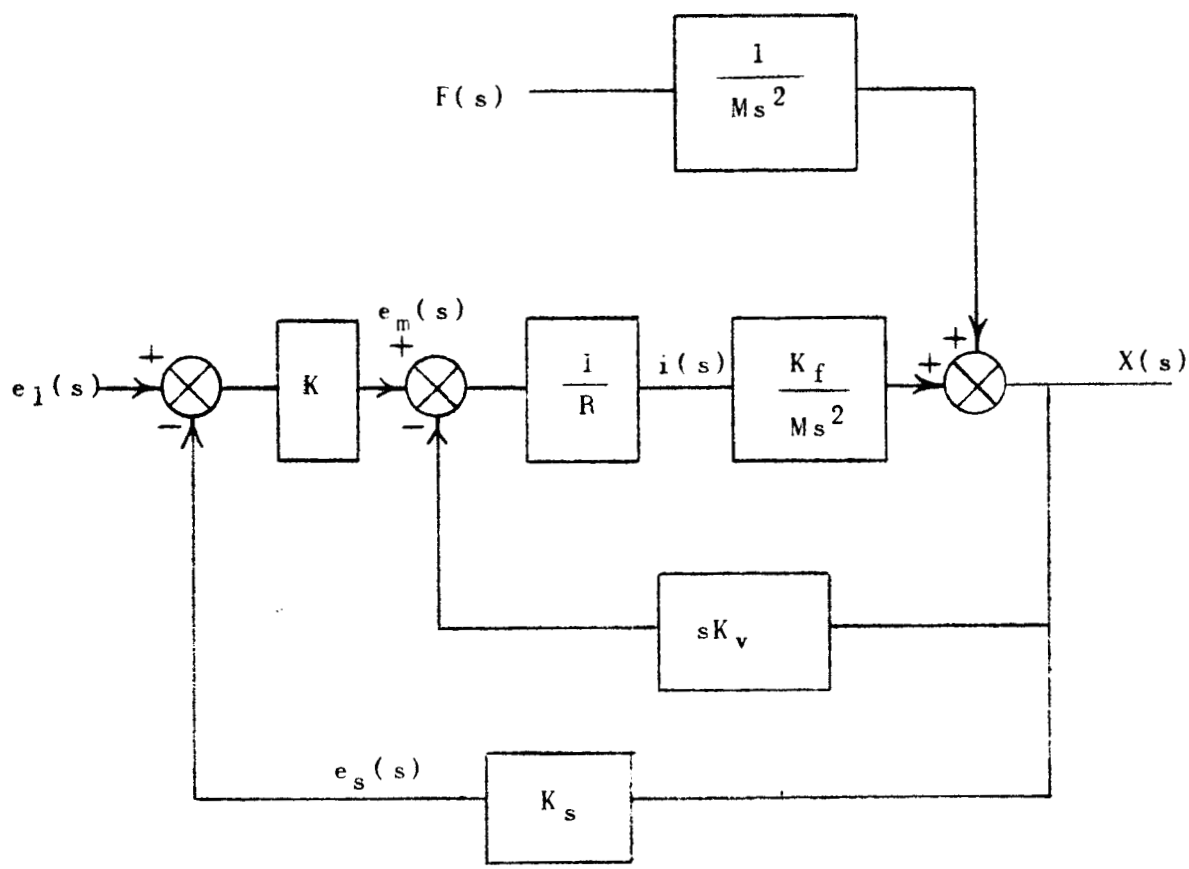

Figure 2-1

Block Diagram of System Neglecting Viscous Friction

steady-state position in the absence of a model force.

The open loop transfer function with respect to input position is

$$\frac{x(s)}{e_1} = \frac{K\,K_{f/MR}}{s\left(s + \frac{K_f K_v}{MR}\right)} \tag{2-8}$$

Since this transfer function contains an integration, the zero force position corresponds to the positioning voltage because the steady-state error of a type 1 system is zero for a step input.

A relation between motor current and model aerodynamic force can be derived by combining Eqs. (2-3), (2-6), and (2-7). Thus,

$$i(s) = \frac{K_v}{MR} \frac{\left(s + \frac{K\,K_s}{K_v}\right)}{s^2 + \frac{K_f K_v}{MR} s + \frac{K\,K_s K_f}{MR}} F(s) \tag{2-9}$$

Under steady-state conditions an aerodynamic force can be represented by a step function of magnitude F. Using this force and applying the final value theorem to Eq. (2-9) results in

$$i_{ss} = - \frac{F}{K_f} \tag{2-10}$$

where the step of force was considered negative. Recalling Eq. (2-2), we see that

$$F_m = - F \tag{2-11}$$

Thus the model force is equal and opposite to the motor force, and the aerodynamic force is proportional to the steady-state motor current with the motor force constant being the constant of proportionality.

Another very important relation that is essential to the design of the system is the equation relating the steady-state displacement to the system parameters. The steady-state displacement must be known in order to choose the sensors and because the cross-coupling of the forces will be related to displacement.

Figure (2-1) shows that the transfer function relating position and input force is

$$\frac{x(s)}{F(s)} = \frac{1}{M} \quad \frac{1}{s^2 + \frac{K_f K_{vs}}{MR} + \frac{K_s K K_f}{MR}} \tag{2-12}$$

Again the force input is assumed to be a step of magnitude F, and applying the final value theorem yields

$$x_{ss} = \frac{R}{K K_s K_f} F \tag{2-13}$$

Referring again to Fig. (2-1) we see that the steady-state displacement is inversely proportional to the loop gain constant. Since gain is relatively easy to obtain (within limits imposed by stability considerations), the displacement is under the designer's control.

Preliminary calculations of the steady-state

displacement can be made by assuming values for the system parameters. The approximate closed loop resonant frequency of the system can be obtained from Eq. (2-12) as

$$\omega_n^2 = \frac{KK_sK_f}{MR} \tag{2-14}$$

and the loop gain constant is

$$\text{Gain} = \frac{KK_sK_f}{R} \tag{2-15}$$

Therefore

$$\text{Gain} = M\omega_n^2 \tag{2-16}$$

By combining Eqs. (2-13) and (2-16) the steady-state displacement can be expressed as

$$x_{ss} = \frac{F}{M\omega_n^2} \tag{2-17}$$

If the closed loop resonant frequency is 30 Hz and the supported mass is estimated to be 8 pounds (mass) or 0.25 slug, a model force of 0.5 pound produces a displacement of 0.000675 inch or 0.675 mil. Since the maximum model force of interest is 0.5 pound this is the maximum displacement if the assumptions are correct. As the reader is aware, these are just preliminary calculations. A designer may simultaneously control loop gain and bandwidth within practical limits through compensation to meet development specifications.

In the derivation of the previous block diagram, force was considered an output disturbance while the input was the positioning voltage. Since using the aerodynamic force as the input seems more logical than using the bearing positioning voltage, Fig. (2-1) can be rearranged as shown in Fig. (2-2). This block diagram has the aerodynamic force as the input and displacement as the output. If the positioning voltage is disregarded (assumed to be zero), the block diagram can be reduced to that of Fig. (2-3).

ANALYSIS INCLUDING VISCOUS FRICTION

In the previous analysis any viscous friction due to the gas bearing was considered to be negligible, but a complete analysis for dynamic considerations must consider the possibility of an appreciable amount of viscous friction (data supports the conclusion (2, 3)).

To derive the appropriate relationships, Eq. (2-1) is modified to include the effect of viscous friction which is a function of the time rate of change of position. Thus,

$$F + F_m - K_b\dot{x} = M\ddot{x} \tag{2-18}$$

where K_b is the coefficient of viscous friction. Taking the Laplace transform and solving for the displacement yields

$$x(s) = \frac{F(s) + F_m(s)}{Ms\left(s + \frac{K_b}{M}\right)} \tag{2-19}$$

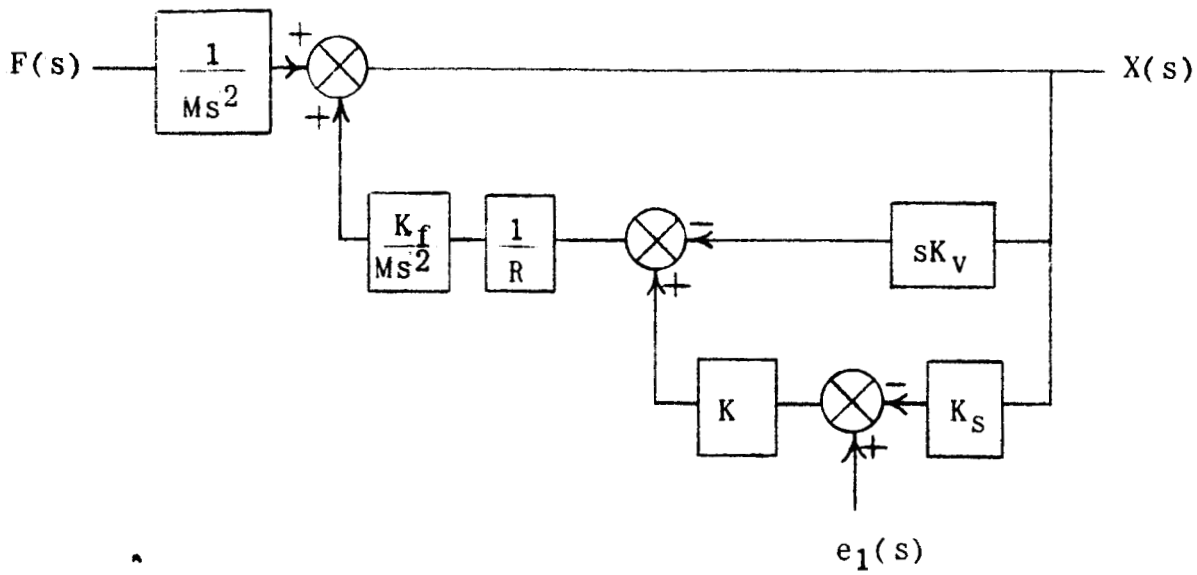

Figure 2-2

Block Diagram Showing Aerodynamic Force as the Input

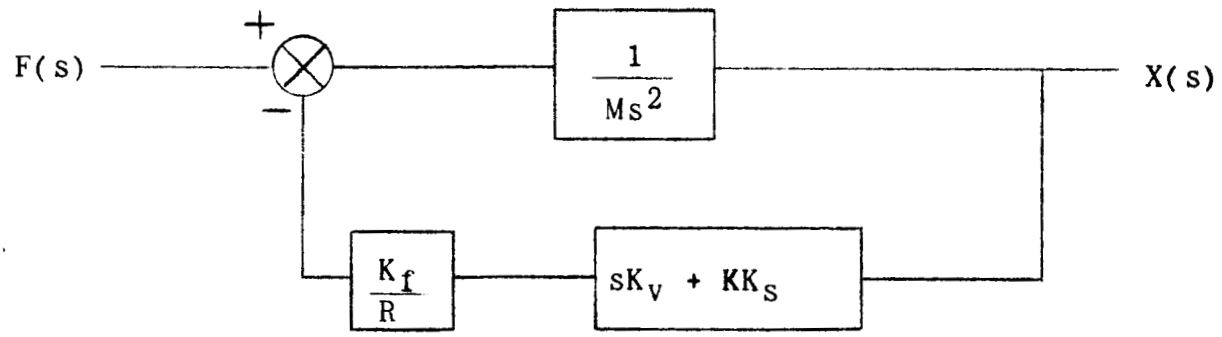

Figure 2-3

Simplified Block Diagram with Aerodynamic Force Input

Applying Eq. (2-2) yields

$$x(s) = \frac{F(s) + K_f i(s)}{Ms(s+\frac{K_b}{M})} \tag{2-20}$$

The other elements of the block diagram are not changed, so the block diagram of Fig. (2-4) can be drawn. This block diagram can be altered and reduced as before to the diagram of Fig. (2-5).

Figure (2-5) can be used to obtain the closed loop relation between displacement and force. Thus

$$\frac{x(s)}{F(s)} = \frac{1}{M} \frac{1}{s^2 + \frac{1}{M}(K_b + \frac{K_v K_f}{R})s + \frac{KK_s K_f}{MR}} \tag{2-21}$$

The steady-state displacement for this case can be obtained by again assuming a step of magnitude F for the force and applying the final value theorem to obtain

$$x_{ss} = \frac{R}{KK_s K_f} F \tag{2-22}$$

Thus, the steady-state displacement is independent of the viscous friction, and the result of Eq. (2-13) is obtained. This was to be expected since the viscous friction is proportional to the time rate of change of the displacement which is zero in the steady state.

Although viscous friction does not affect the steady-state operation of the system, it can easily be shown that

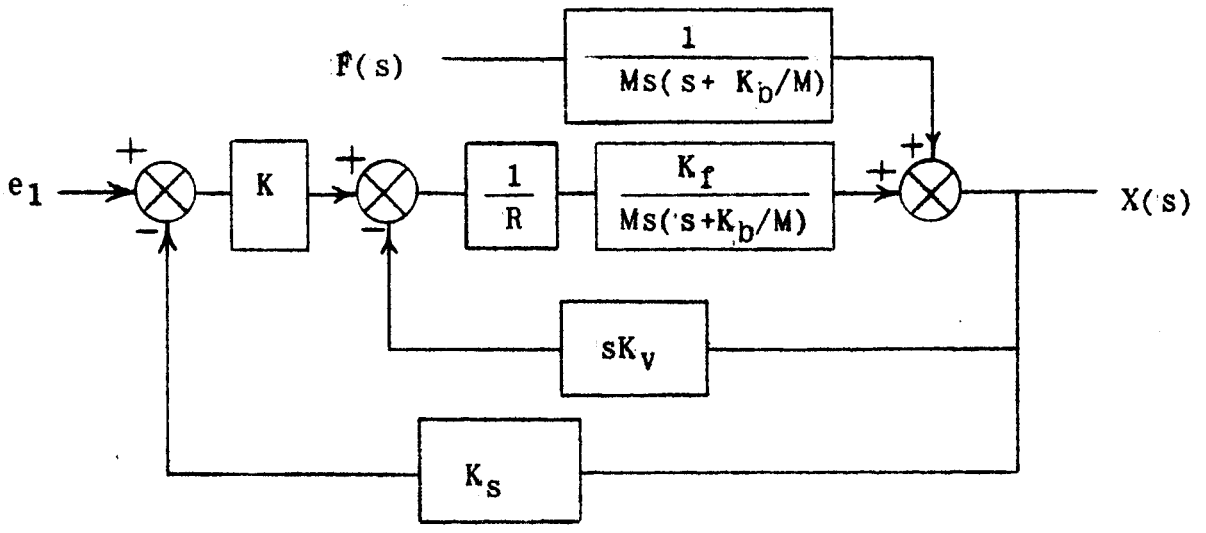

Figure 2-4
Block Diagram with Viscous Friction Included

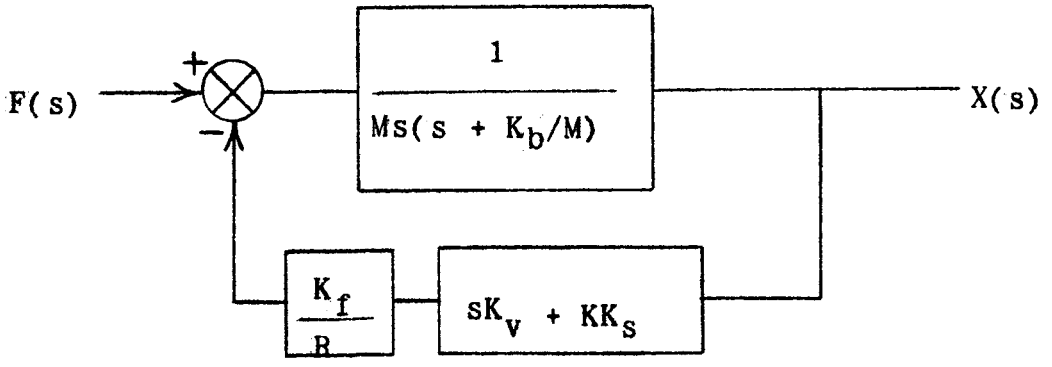

Figure 2-5
Simplified Block Diagram with Viscous Friction Included and with Force as Input

it does affect the transient behavior and stability. The loop gain of the system disregarding viscous friction is

$$(GH)_{\substack{\text{without viscous}\\\text{friction}}} = \frac{K_f K_v}{MR} \frac{s + \frac{KK_s}{K_v}}{s^2} \qquad (2\text{-}23)$$

from Fig. (2-3). The loop gain including viscous friction is

$$(GH)_{\substack{\text{with viscous}\\\text{friction}}} = \frac{K_f K_v}{MR} \frac{s + \frac{KK_s}{K_v}}{s(s+\frac{K_b}{M})} \qquad (2\text{-}24)$$

from Fig. (2-5). The root-locus representations of Eqs. (2-23) and (2-24) are shown in Figs. (2-6) and (2-7) respectively. It can be seen from these diagrams that the analysis including viscous friction shows that viscous friction improves the relative stability of the closed-loop system for a given loop gain constant.

Because cross-coupling is a function of displacement, it would be desirable to eliminate the steady-state displacement. With the system described by Eqs. (2-23) or (2-24), this would only be possible with an infinite gain constant. The system can, in theory at least, be modified to eliminate the steady-state displacement by inserting an integration in the feedback loop of Figs. (2-3) or (2-5). If this could be accomplished in the physical system, the steady-state displacement would be zero for any force input within the limits of the system. This should be a subject for future research.

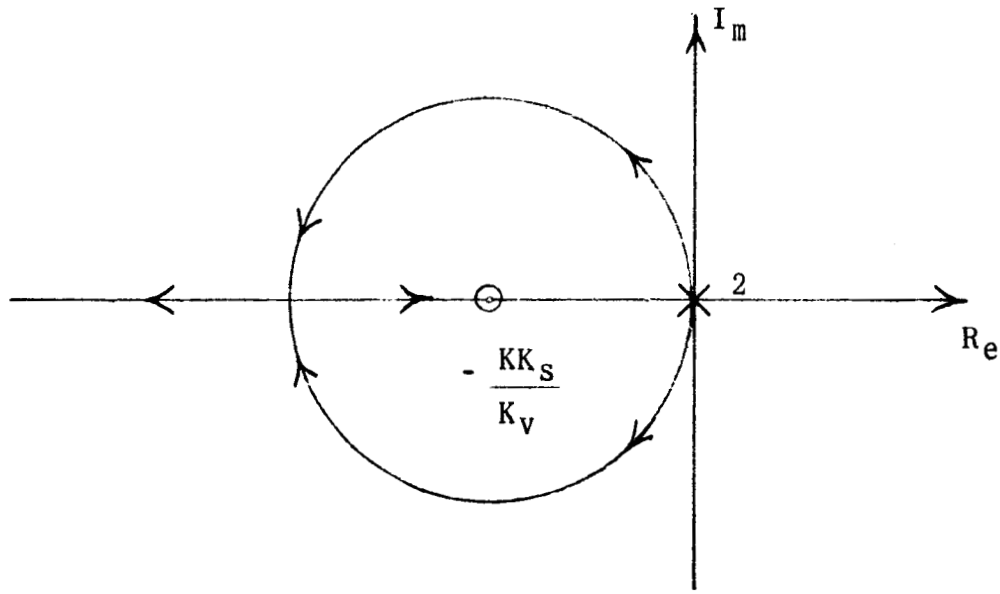

Figure 2-6

Root Locus of System Disregarding Viscous Friction

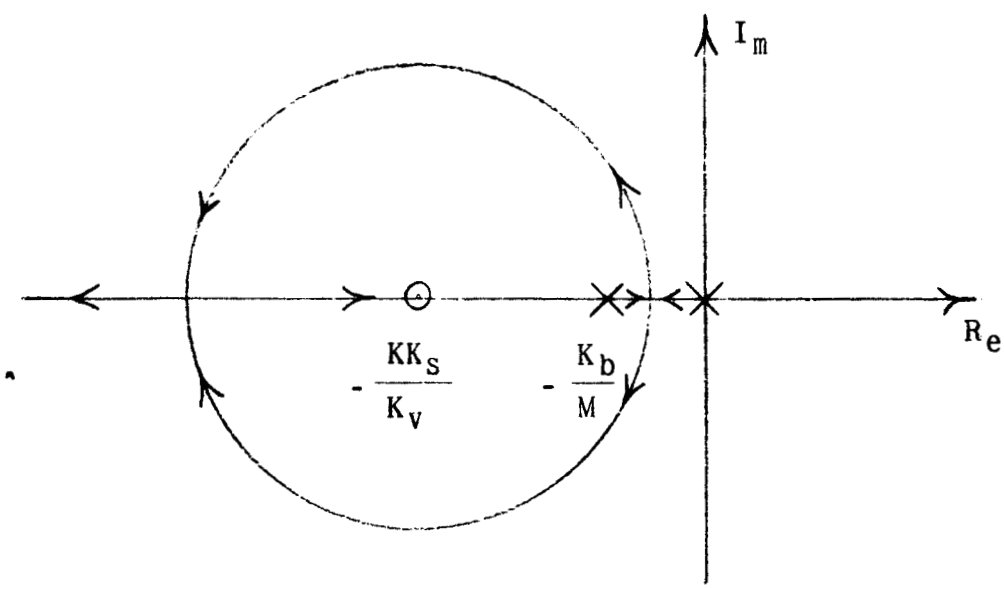

Figure 2-7

Root Locus of System Including Viscous Friction

In all of the previous analysis, resonances in the various mechanical parts of the system have been disregarded. Thus, the loop gain will probably be influenced by factors in the actual model that have not been considered. These factors will be considered in Chapter V where actual data are used for final design.

The analysis presented in this chapter presents a theory for force measurements if the assumptions are valid. The problem areas and components which need detailed consideration to build an actual system are:

1. Motors
   - A. Cross-coupling between perpendicular forces in the plane and pitch moment
   - B. Motor force rating of 0.5 pound
   - C. Drift sensitivity
2. Sensors
   - A. Resolution
   - B. Mechanical clearance
   - C. Production of undesirable forces
   - D. Time constants
   - E. Cross-coupling
3. Amplifiers
   - A. Time constants
   - B. Drift stabilization

4. Mechanical

   A. Resonances of string, motor arm, and sensor mountings

All of these topics are considered in the chapters which follow.

CHAPTER III

MOTOR DESIGN

After the original idea for the system had been conceived and the implementation of the idea had begun, it was realized that the single most critical component of the control system was the servo motor. This is true because the amount of cross-coupling between the measurements is primarily determined by the amount of cross-coupling generated by the servo motors and because certain types of motors have "off center forces" (8) which can result in an open loop unstable system. Such a system is undesirable because it would, at best, be conditionally (Nyquist) stable and because these forces enter into system error considerations. If the maximum force were applied in one direction, 0.5 pound, and the minimum force were applied in the other direction, 0.005 pound, a cross-coupling force generated by the servo motors in the first direction of 1% of maximum force would be equal to the applied force in the other direction. This would make data reduction far more difficult than if the cross-coupling were negligible.

In addition to the minimization of cross-coupling, the motors must meet maximum force requirement of 0.5 pound in each of the coordinate directions. Two servo motors were used to provide the necessary force in each direction because

two motors were required to null the torque component, and it was more economical to build four identical motors. Therefore, each servo motor must be capable of providing half the maximum force or 0.25 pound. Each servo motor must be capable of providing this maximum force for the full period of operation without damage or drift due to overheating. A maximum run-time for the system will be on the order of several minutes.

For the reason stated above, it was decided that the system should be made open-loop stable. This meant that a type of motor had to be adopted which would exert no force when no current was applied. In order to accomplish this, using magnetic principles, the flux path of either the field or the armature had to be through air rather than through a magnetic material.

Two types of motors were investigated theoretically before a final choice was made. The first type of motor that was considered was the loudspeaker type of motor (also called shaker type for vibration). In this type of motor the force is produced by the interaction of the fields of a permanent magnet and an electromagnet. The frame of the electromagnet is concentric with the permanent magnet, and the permanent magnet is mechanically connected to the moveable arm of the balance system. This type of motor has the distinct advantages of being easy and inexpensive to construct, but the theoretical investigation revealed that

the cross-coupling between the perpendicular forces was a first-order effect with respect to displacements in the plane of the measurements (6). Since cross-coupling is very undesirable, this type of motor was not used for the prototype.

Another type of motor that was investigated was a motor derived from work that has been done on magnetic support systems (7, 8). Magnetic support systems have been the subject of extensive research at the University of Virginia. The purpose of the previous work was to support and position a small piece of magnetic material, and apparently, this is the first application of this theory to anything other than a magnetic support system. A brief treatment of some of the theory governing the operation of this type of motor is presented in Appendix A.

In simplest terms the operation of this type of motor may be explained with the aid of Fig. (3-1). In the diagrams of Fig. (3-1) the permanent magnet, which is mounted vertically as shown on the magnet and sensor support arm (see Fig. (1-1)), is in the fields of two electromagnets with their poles oriented as shown. For the only two possible orientations of the poles of the electromagnets (the electromagnets are connected in series with opposing fields), the directions of the forces are as shown. As shown in Appendix A, the force on the permanent magnet is perpendicular to the magnetic moment when the angle between the moment

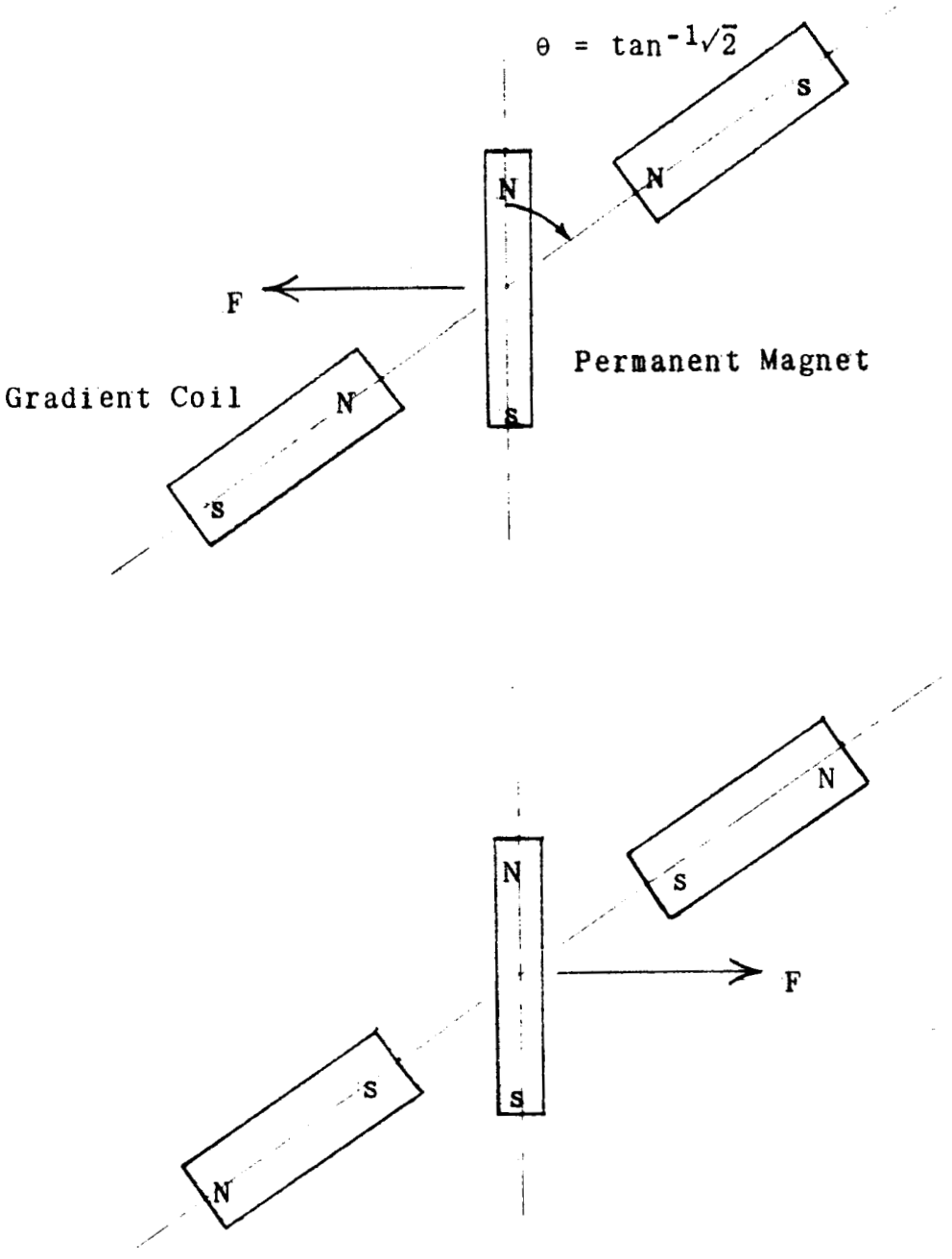

Figure 3-1

Operation of Servo Motors

and the axis of symmetry of the gradient coils is $\tan^{-1}\sqrt{2}$. Furthermore, the force is in the plane formed by the axis of symmetry of the gradient coils and the vertical line intersecting the axis. Thus, it takes two coils and a permanent magnet to make one motor, but a second motor with its force perpendicular to the first can be made by the addition of two coils with their axis of symmetry perpendicular to the axis of symmetry of the first two. A picture of a completed motor for the prototype is shown in Fig. (3-2). This shows the orientation of the magnet and coils for the x and y-direction motors of one side of the balance system.

Two sources of cross-coupling forces are present in the coil axis alignment. Jenkins and Parker (7) have shown that a force is generated parallel to the direction of the moment which is coupled to the desired force to the first order in the error of the angle between the gradient coil axis and the moment. This force component has no effect on the balance system since the moment is vertical (in the z-direction of the system coordinates), and therefore, the force works against the gas bearing. The second cross-coupling force is due to misalignment of the motors with respect to the system coordinates. This is a first order effect also and can only be minimized with very careful alignment of the motors.

The motors shown in Fig. (3-2) were not designed with the aid of the design equation that was developed in

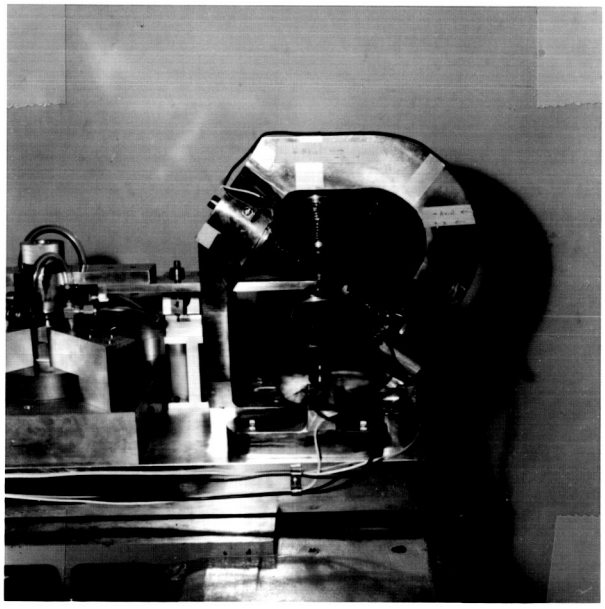

Figure 3-2
Completed Motor

Appendix A because experiment showed that this equation was not accurate enough. The motors were designed on the basis of the field due to a single circular loop and measurements that were made on an experimental model.

The experimental model was constructed using a permanent magnet that was available. This magnet was made of Alnico V and was two inches long by 1/4 inch diameter. The gradient coils were wound with 20 turns of #20 magnet wire with a mean diameter of 2.5 inches and a spacing between coils of 3.25 inches. The force exerted by this motor for various coil currents was determined by supporting the permanent magnet on a pan balance.

In order to obtain an analytical expression that could be easily minimized with respect to the various parameters, Eqs. (A-22) and (A-24) of Appendix A were combined to give:

$$|F| = 2.66 \times 10^{-6} \frac{M_o V I a^2 Z_o}{(a^2+Z_o^2)^{5/2}} \qquad (3\text{-}1)$$

This is the equation for the force on a moment due to two single turn circular loops oriented as shown in Fig. (3-3). When this equation was multiplied by the number of turns and the values of the parameters substituted, it was found that the force was slightly less than two orders of magnitude greater than the force determined by the experiment described above. On the basis of these results it was

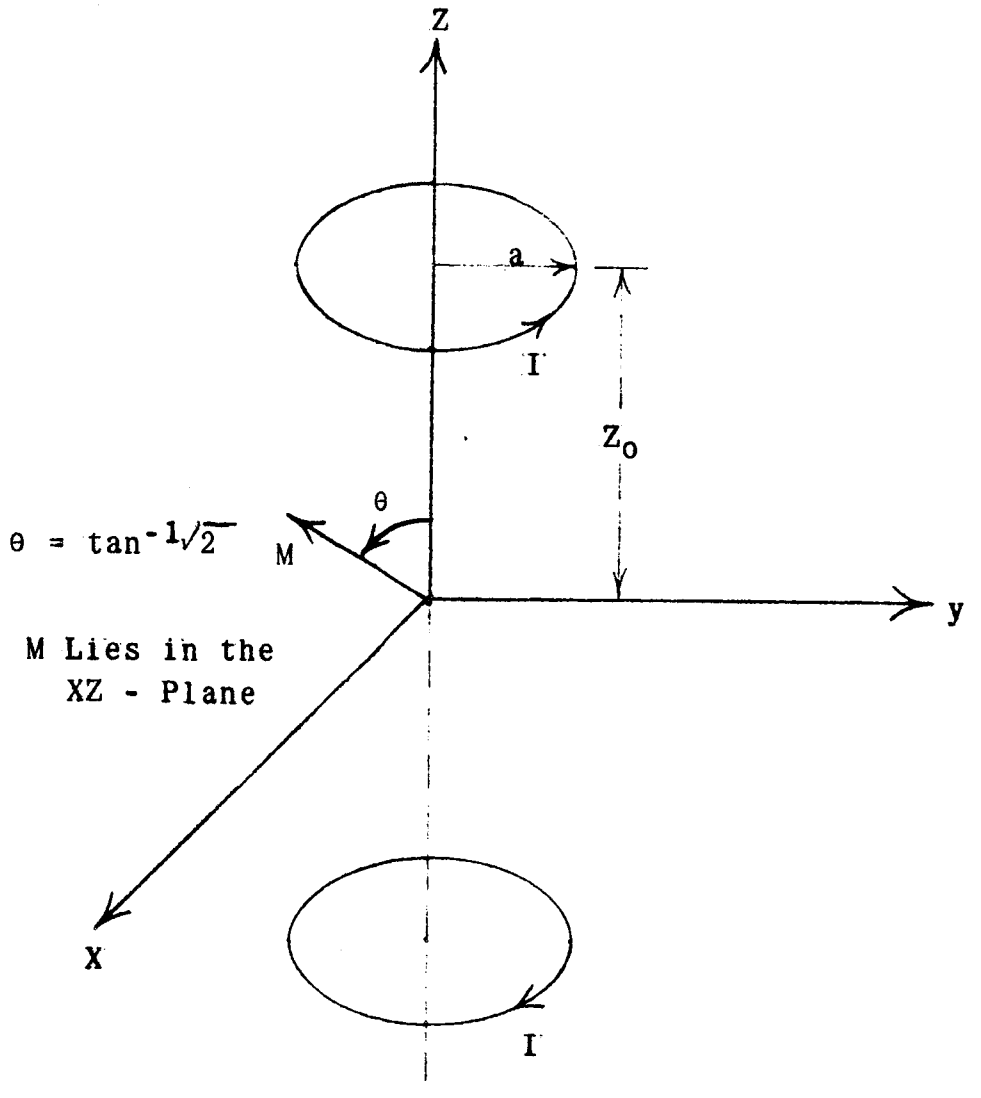

Figure 3-3

Single Loop Gradient Coil Motor Geometry

decided that the number of turns of the final design should be 100 times the number indicated by the solution of Eq. (3-1).

By trial and error investigation of Eq. (3-1) and demagnetization and energy produce curves furnished by a manufacturer (9), an optimum magnet size was chosen on the basis of the product of moment and volume. The magnet chosen was made of Alnico V and was 2.25 inches long with a diameter of 0.5 inch.

Once the magnet size had been chosen, the coil spacing from front face to front face could be determined graphically. On the basis of this dimension, a mean coil spacing was chosen for use in the solution of Eq. (3-1). The mean coil spacing that was chosen was 2.75 inches. Since the mean coil spacing is fixed by geometric considerations, Eq. (3-1) can be used to determine the coil radius that will give the maximum force. Taking the partial derivative of Eq. (3-1) with respect to the radius and setting the result equal to zero gives:

$$a = \frac{2Z_o}{\sqrt{6}} = 1.12 \text{ inches} \qquad (3\text{-}2)$$

This is the mean coil radius that will be used in the design.

The remainder of the motor design consists of finding the shape and dimensions of the coils that will meet the mean spacing and radius specifications that have been determined. After this is completed, the number of turns, size

of wire, and current can be determined and the resulting design can be checked by substitution into Eq. (3-1) and application of the multiplication factor that was experimentally determined.

In order to insure that the coils can be fitted with the correct geometry, it is necessary to determine the angle between the axes of symmetry of the coils so that the coils can be sized and shaped to prevent crowding. This angle can be determined with the aid of Fig. (3-4). The vectors, $\hat{V}_1$ and $\hat{V}_2$, are unit vectors in the same directions as the coil axes. They may be expressed as:

$$\hat{V}_1 = \hat{i} \sin 54.7^\circ + \hat{j}0 + \hat{k} \cos 54.7^\circ \qquad (3\text{-}3)$$

$$\hat{V}_2 = \hat{i}\, 0 + \hat{j} \sin 54.7^\circ + \hat{k} \cos 54.7^\circ \qquad (3\text{-}4)$$

If β is defined as the angle between the two vectors, then

$$\beta = \cos^{-1} \frac{\hat{V}_1 \cdot \hat{V}_2}{|\hat{V}_1||\hat{V}_2|} = 70.2^\circ \qquad (3\text{-}5)$$

With this angle and the mean coil spacing, a graphical determination of the size and shape of the coils can be made, keeping in mind the mean coil radius specification. The shape that was chosen is shown in Fig. (3-2), and the dimensions are:

Coil spacing (face to face) - 2.25 inches

Outside coil radius (magnet side face) - 0.75 inch

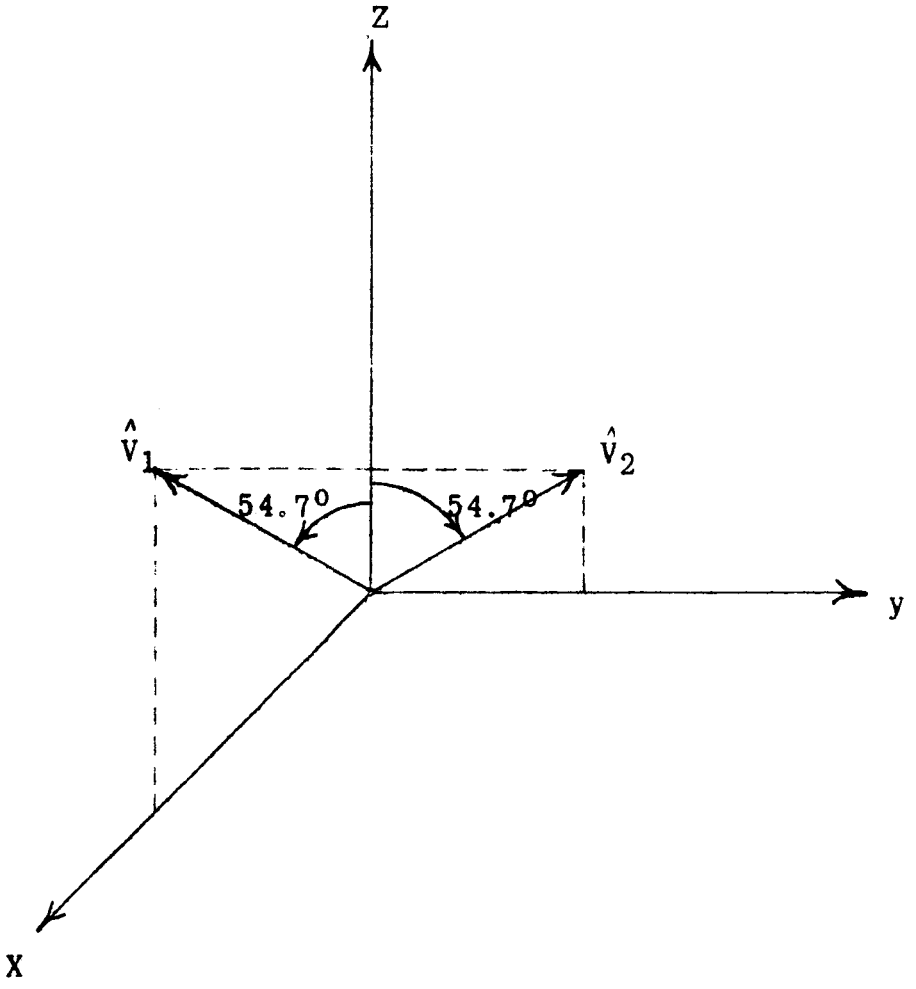

Figure 3-4

Vector Determination of Angle Between
Gradient Coil Axes

Outside coil radius (opposite face) - 1.75 inches

Inside coil radius - 0.5 inch

Coil length - 1.5 inches

The values of the parameters were substituted into Eq. (3-1), and the equation was solved for the NI or amp-turn product. When the multiplication factor was included, the result was 3000 amp-turns for a force of 0.25 pound. After consideration of space available on the coil forms, current requirements, wire size, and heating due to I^2R loss, it was decided to use 1000 turns of #20 enameled copper wire on each motor coil. This fixed the maximum coil current at three amps.

The four motors were constructed to the specifications given by the design. In order to determine the motor constant, data was taken by applying a known force to the shaft attached to the gas bearing and then increasing the current through the gradient coils until the gas bearing moved from its mechanical stop. The results of this experiment were sufficiently accurate to prove the design. The results are shown in Fig. (3-5) in the form of force data. This figure shows that the design was quite accurate despite its approximate nature because extrapolation of the data indicates that a force of 0.25 pound requires a coil current of 2.62 amps. Since the resistance of the two series coils was 9.4 ohms, the power required by the motors was found to be of a level that could be delivered by power transistors. Thus, the

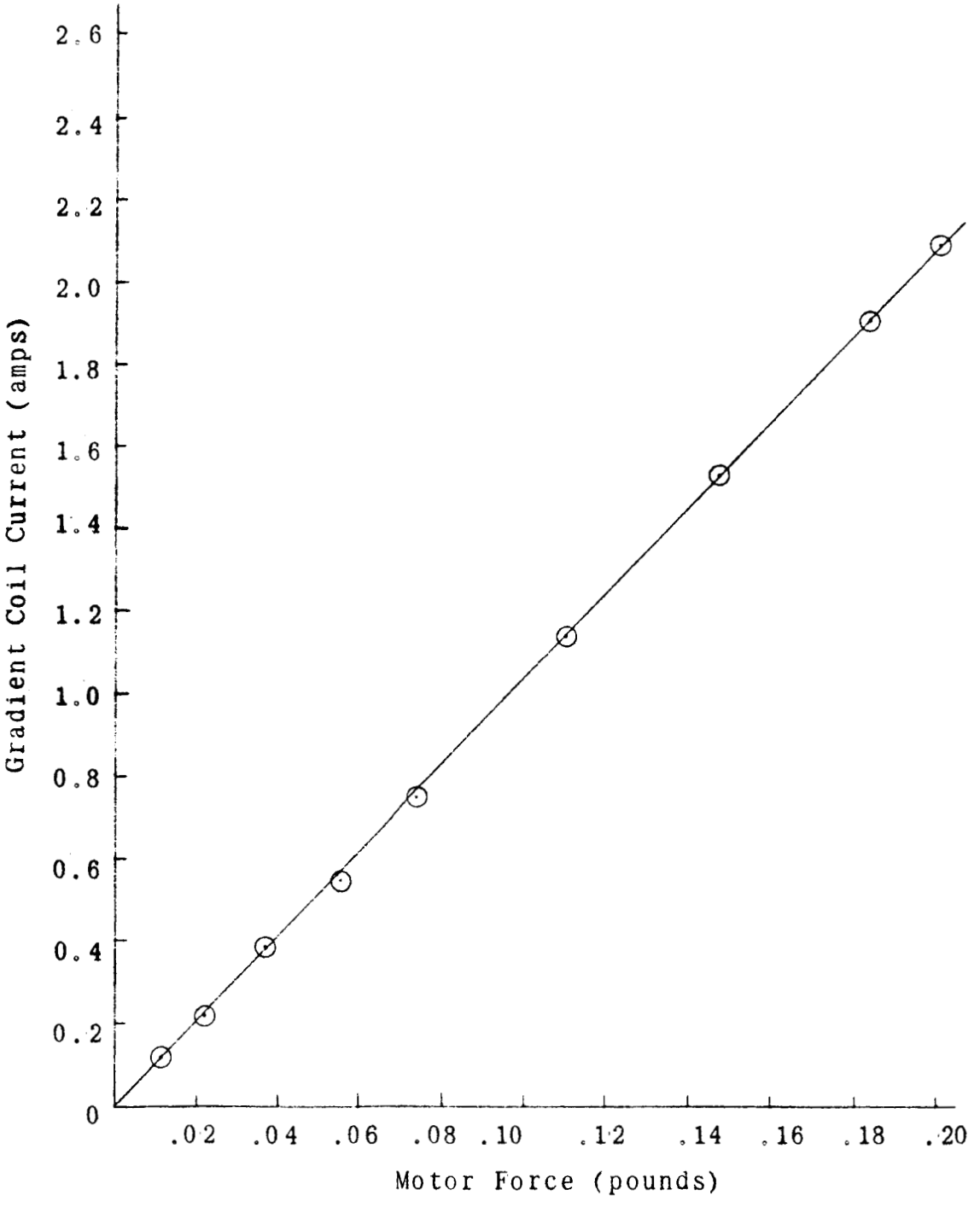

Figure 3-5

Servo Motor Force Characteristic

servo amplifiers that are required have a power specification that can be realized practically.

The inductance of one of the motors was measured to validate the assumption that the inductance was negligible at the frequencies of interest. The measured inductance was 6.8 millihenries. At 30 Hz, the inductive reactance of a motor is 1.3 ohms which can be considered negligible since the system response drops rapidly beyond 30 Hz.

CHAPTER IV

COMPONENT DESCRIPTION

SENSORS

It was shown in Chapter II that the steady-state displacement error for maximum force input was slightly greater than 0.0005 inch for the assumed parameters. Since the steady-state displacement is proportional to the force input, the displacement for minimum force input should be slightly greater than 5 micro-inches. Thus the first requirement for the sensors is a resolution of a few micro-inches.

The second requirement that the sensors must meet is a clearance specification. Since the sensors are being used to sense displacements in perpendicular directions, sufficient clearance must be provided so that the sensor perpendicular to the direction of the applied force will not tend to limit the displacement. This establishes the clearance that is needed theoretically, but the practical problem of aligning the system requires that a considerably greater amount of clearance be provided.

The third requirement is a bandwidth of at least ten times the crossover frequency of the mechanical part of the system. This was assumed in Chapter II and is necessary to prevent the sensor from adversely affecting the stability of the system. A related requirement determines the

excitation frequency that may be used by the sensors. This frequency should be many times the crossover frequency of the system in order to prevent the portion of the excitation that remains after filtering from producing motion in the system.

Since there are two degrees of freedom in the system there are two further requirements that the sensors must meet which are less obvious but just as important as the ones already considered. The first of these is concerned with the generation of forces by the sensors in the direction in which displacement is being sensed. Any force of this type which is generated should be much less than the smallest force of interest, 0.005 pound, so that calibration will not be affected. The second concerns generation of forces perpendicular to the direction in which displacement is being sensed. A force of this type leads to a false readout as does a force generated in the direction of sensing, but it could also lead to an instability due to open loop poles in the right half of the complex frequency plane because of the cross-coupling of the servos in the two directions.

The last special requirement that the sensors for this system must meet is the requirement that the sensor constant should be relatively independent of small displacements perpendicular to the sensing direction. A change in gain anywhere in the loop changes the stiffness of the servo.

Furthermore, a high gain constant is a good property, but additional gain can be obtained through amplification.

After consideration of these special requirements as well as availability, price, reliability, and ease of installation, it was decided that linear variable differential transformers (abbreviated LVDT) would be used for the three displacement sensors.

The LVDT converts mechanical displacement into a voltage that is proportional to the displacement (10). It consists of a magnetic core that is attached to the movable member and a body which contains three separate windings as shown schematically in Fig. (4-1). The primary is energized with an alternating current, and the position of the core determines the amount of coupling to the two secondary windings. The secondary windings are connected in series opposition, so the output is the difference between the voltages induced in the two windings. At the point where the two induced voltages are equal there is a null or zero output position. As the core moves from one side through the null position, the phase of the output shifts by 180°. The output to the system is obtained by phase detection, rectification, and filtering. Thus the output to the system is a direct current, the voltage of which is proportional to the displacement from null position and the polarity of which is determined by the side of null position that the core is on.

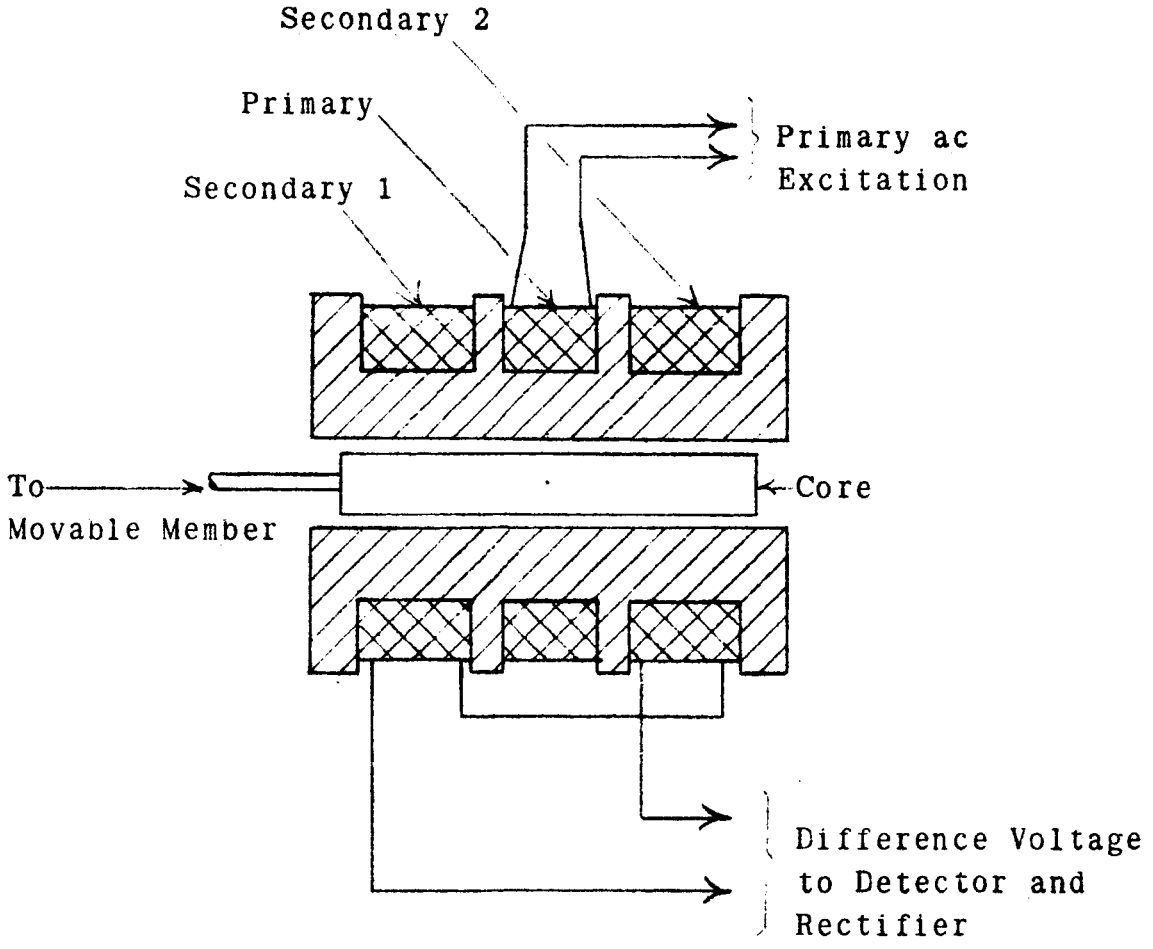

Figure 4-1

Linear Variable Differential Transformer

LVDT's are commercially available in two types according to construction. The first has a separate transformer and carrier-demodulator assembly, and the second type is wholly contained in one unit. The first type is usually a better (and more expensive) LVDT because space limitations do not require the sacrifice of ripple and drift tolerances. Both types were used in the balance system because two of the self-contained units were available at no cost. The first type was used for sensing the x-direction displacements while the two self-contained units were used to sense y-direction displacements.

The specifications of the sensors as provided by the manufacturers (11, 12) are listed below:

X-DIRECTION SENSOR

LVDT

Manufacturer - Schaevitz Engineering Company

Model Number - 010MS-L

Linear Range - 0.010 inch each side of null

Sensitivity - 4.6 mv/0.001 inch/volt input at 20,000 Hz with 0.5 megohm load

Radial Clearance - 0.008 inch each side of center

Linearity - $\pm$ 0.5% of maximum linear output

CARRIER-AMPLIFIER-DEMODULATOR UNIT

Manufacturer - Schaevitz Engineering Company

Model Number - CAS-20,000

Carrier Frequency - 20,000 Hz

Frequency Response - D. C. to 250 Hz ± 1 db

Ripple - 25 mv-rms maximum

Output Impedance - 1000 ohms maximum

Gain Stability - 0.5% (after 15 minutes)

Sensitivity - A. C. amplifier gain adjustable from 1 to 100

Transducer Excitation - 1.25 volts-rms, 0.5 va

Overall Maximum Sensitivity - 575 volts/inch

Y-DIRECTION SENSOR

Manufacturer - G. L. Collins Corporation

Sensitivity - 44 volts/inch

Radial Clearance (after machining) - 0.010 inch each side of center

Carrier Frequency - 4,000 Hz

The remaining specifications are similar to those given above.

The last special requirement placed on the sensors for this system, low cross-coupling, was easy to check when one of the units had arrived. The sensor was mounted rigidly to a frame, and the core was attached to a micrometer which was attached to the frame. Then the output as a function of displacement was recorded for the core displaced to one side of the sensor barrel. Then the experiment was repeated with the core displaced to the other side of the barrel. The results of this experiment are plotted in Fig. (4-2). The fact that the null position is not the same for both cases

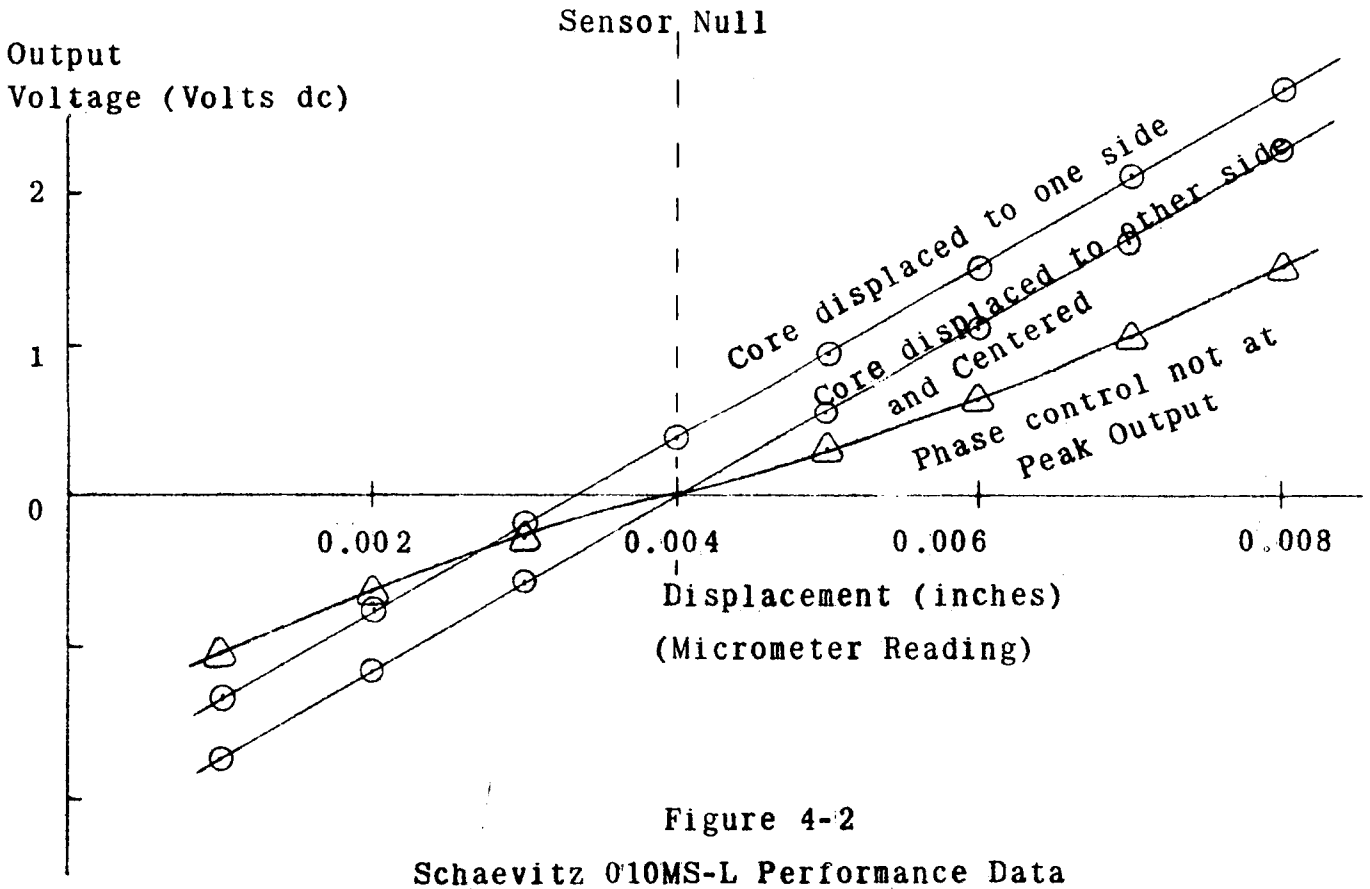

Figure 4-2

Schaevitz 010MS-L Performance Data

is not significant because the system output (force reading) is independent of the null position, and, in addition, it may be explained as an error in the experiment. The sensor was attached to the frame by means of a screw which had to be loosened when the core position with respect to the radial direction was changed. When the screw was again tightened, it was not tightened to the same degree resulting in a small displacement in the sensing direction. This figure does show that the gain is independent of radial displacement within the limits of this experiment. The third curve on Fig. (4-2) is data that was taken when the phase control on the carrier-amplifier-demodulator unit was set at some position other than that which gave maximum output. This shows the importance of insuring that this control is properly adjusted.

Information furnished by the manufacturer shows that the LVDT with an excitation of 20,000 Hz exerts a force in the sensing direction which is less than one milligram (13). Since the smallest force of interest is 0.005 pound or 2.2 grams, the core pull is negligible.

AMPLIFIERS

There are three servo loops in the balance system, but there are actually four motors. As stated before (Chapter I) two of the motors provide the x-direction balance force by working in parallel. Since the four motors had identical characteristics, it seemed more economical to design four identical amplifiers and have the two x-direction amplifiers

driven by the same sensor output. This was more economical in terms of design time, power supply cost, and ease of maintenance.

The first requirement that the amplifiers must meet is a frequency response specification. The amplifiers ideally would have a relatively flat response from dc to a frequency at least ten times the crossover frequency of the mechanical part of the system. Making the cutoff frequency of the amplifier so high with respect to the cutoff frequency of the mechanical part of the system minimizes the effect of the amplifier time constants on the stability of the system.

As previously stated, the motors require 2.62 amps to produce 0.25 pound force as required by the system. Since the y-direction motors must produce a force in both the positive and negative y-directions, the amplifiers must be capable of providing at least 2.62 amps in both directions through the gradient coils of the motors. The resistance of the gradient coils is 9.4 ohms.

Since dc amplifiers cannot employ capacitor or transformer coupling between stages, one of the most serious design problems for dc amplifiers is the elimination of drift due to changes in bias and operating characteristics of the components. Many schemes have been devised to alleviate this problem, but most of these are limited by practical considerations to relatively low power applications. Since each of the four amplifiers must be able to

provide about 85 watts maximum, it was decided that it was economically impractical to adapt any of the low power configurations.

After consideration of several types of direct-coupled amplifiers, the configuration shown schematically in Fig. (4-3) was chosen. The current source on the right produces three amps (the additional current was added as a design safety factor) regardless of the load or the output of the other current source. The current source on the left is biased to produce three amps with zero input from the sensors. Under this condition there will be no current through the gradient coils, and the force will be zero. As the input voltage becomes positive, the current through the left current source decreases, and the current through the gradient coils is equal to the decrease. The direction of the current will be downward through the coils. If the input voltage becomes negative, the current through the left current source increases, and the current through the gradient coils is equal to the increase; but its direction is now upward through the coils. Thus, this configuration is capable of providing three amps in either direction through the gradient coils.

A schematic diagram of the servo amplifiers is shown in Fig. (4-4). The portion of the schematic enclosed in dashed lines is the constant current generator. It is provided with an entirely separate bias supply in order to

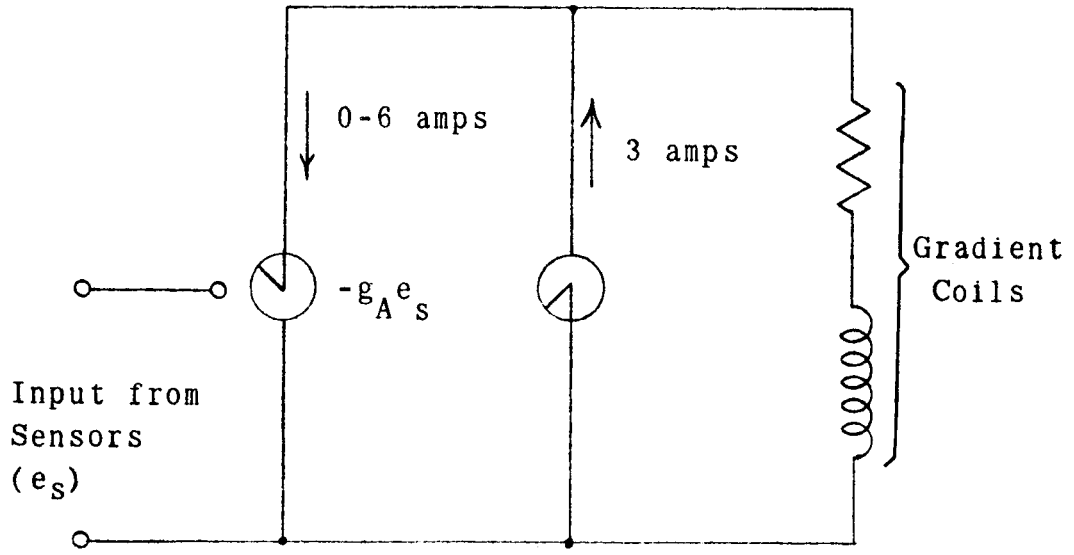

Figure 4-3

Current Source Representation of Power Amplifiers

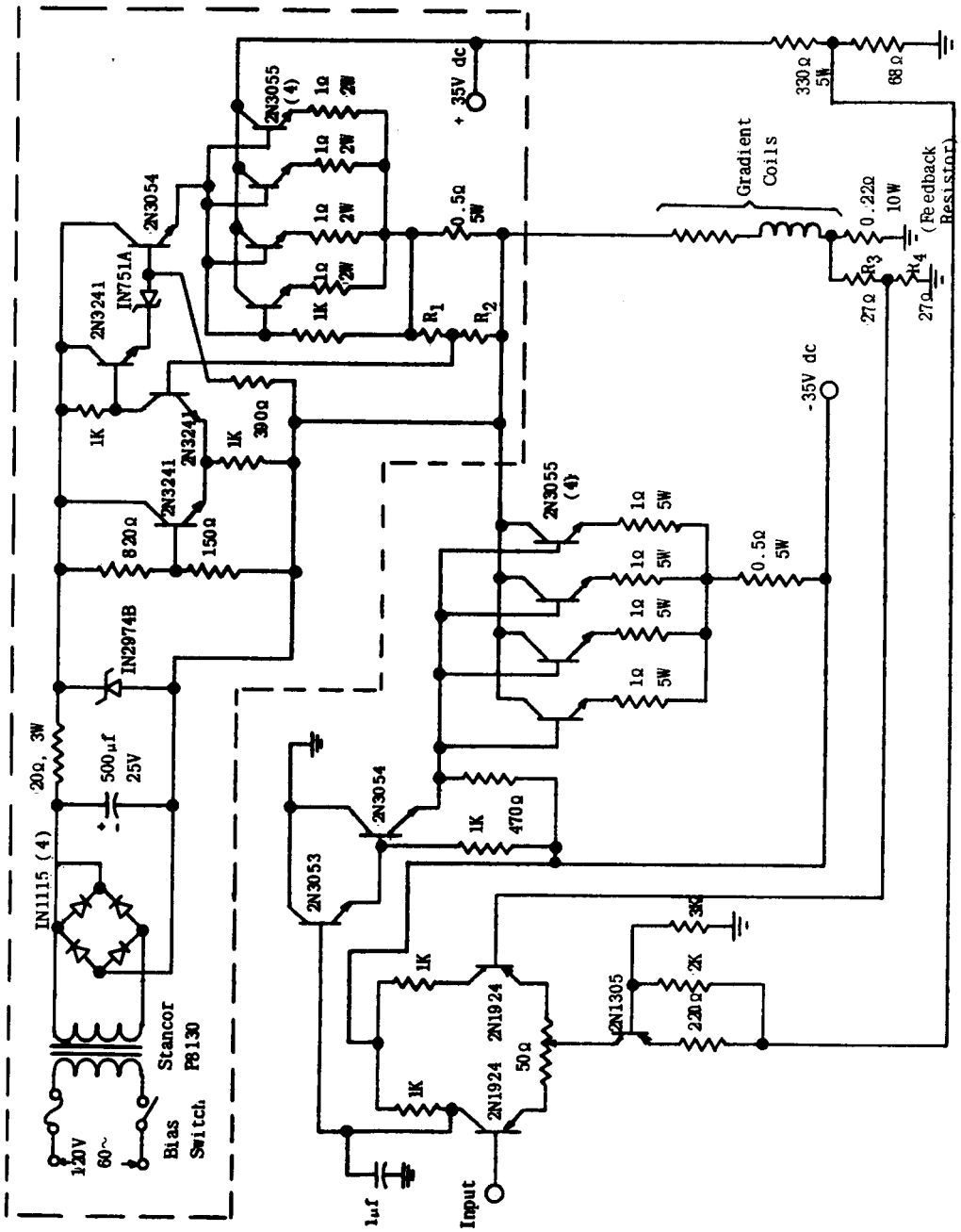

Figure 4-4
Schematic of Servo Amplifiers

isolate it from variations in the main supply which feeds all four servo amplifiers. The amount of current provided by this generator is adjustable over a limited range by adjustment of the values of R_1 and R_2. With the values shown, the source produces three amps.

The remainder of the schematic is the voltage controlled current source. With no voltage at the input, the source is biased to produce three amps. As the input voltage becomes positive, the current provided by this source is decreased; and, as the input voltage becomes negative, the current is increased. Since the sensor output in the x-direction for 0.5 mil displacement is 0.288 volts, the gain of this current source was designed so that an input of 0.288 volts would produce a current of six amps. This gain can be changed by adjusting the values of R_3 and R_4.

The design of the servo amplifiers is a straightforward procedure, and, therefore the details will not be presented. One very important consideration, however, is the power dissipation of the four parallel transistors in the constant current source. When there is no input to the amplifier, the voltage drop across these transistors is 35 volts (ignoring the drop across the emitter resistors and sensing resistor). The total current is three amps, so the power dissipation is 105 watts. However, when the other current source is producing six amps, the drop across the constant current source power transistors is 70 volts (again ignoring

other drops) while the current is still three amps. The power dissipation is now 210 watts. Since the system should be capable of balancing the maximum force in either direction for a sustained period of time, an adequate means of heat dissipation must be provided for this power level.

With no force input to the system, the power dissipation in the power transistors of the two current sources is 210 watts. This is a large standbye consumption, but since run times will be relatively short (several minutes at most) and the system will always have a more than adequate supply of power available, this amount of dissipation is not excessive.

Four servo amplifiers were constructed using the schematic of Fig. (4-4) and mounted on a relay rack as shown in Fig. (6-3). The two power supplies were mounted below the amplifiers and were separated by a switch panel. The switches on the switch panel were arranged so the positive and negative supply voltages could be separately applied to each of the amplifiers for test or servicing purposes.

The four servo amplifiers were designed to work directly from the sensor output, but it was realized that some means of providing compensation for the system would have to be provided. Since compensation can be usually obtained more inexpensively and reliably using R-C networks, it was decided to insert an operational amplifier between the sensor output and the power amplifier input. The design of the

compensation will be discussed in Chapter V.

READOUT

As stated in Chapter I, the force readout is obtained by measuring the currents through the gradient coils, summing or subtracting, and applying suitable calibration. This may be done in any one of several ways, but in this particular case the readout was specified as a voltage proportional to the force being measured. This means that the measurement of the currents and the algebraic operations on these measurements should be performed electronically as a part of the system. It was further specified that a range switch should be included which would divide the specified total range of 0.005 to 0.5 pound into two ranges of 0.005 to 0.05 pound and 0.05 to 0.5 pound with a maximum readout voltage for each range of approximately one volt.

The current through the coils can be determined by measuring the voltage across the feedback resistor of the power amplifiers (0.22 ohm, 10 watt resistor of Fig. (4-4)). At full output, three amps, the drop across this resistor is 0.66 volts which is the right order of magnitude for the high force range since the lift and drag readouts are the sum of two equal voltages.

The readout voltage for the drag measurement can be obtained by summing the voltage drops across the feedback resistors of the two x-direction servo amplifiers. The sum

is most easily obtained with an operational amplifier. The range switching can be accomplished by switching between two values of feedback resistor since the gain of an operational amplifier with feedback is R_f/R_i where R_f is the feedback resistor and R_i is the input resistor (14).

The lift measurement readout voltage can be obtained in the same manner by summing the voltage drops across the feedback resistors of the two y-direction servo amplifiers.

Pitch measurement is accomplished by taking the difference of the voltage drops across the feedback resistors of the two y-direction servo amplifiers. This difference is taken with an operational amplifier also, and the range switch is provided for in the same manner. Since the pitch readout voltage is the difference between two voltages of opposite sign, it will also be of the right order of magnitude.

The schematic diagram of the readout preparation unit is shown in Fig. (4-5). The 4 μf capacitors were placed around the feedback path to remove the undesired measurement of building vibrations which was particularly annoying on the low force range.

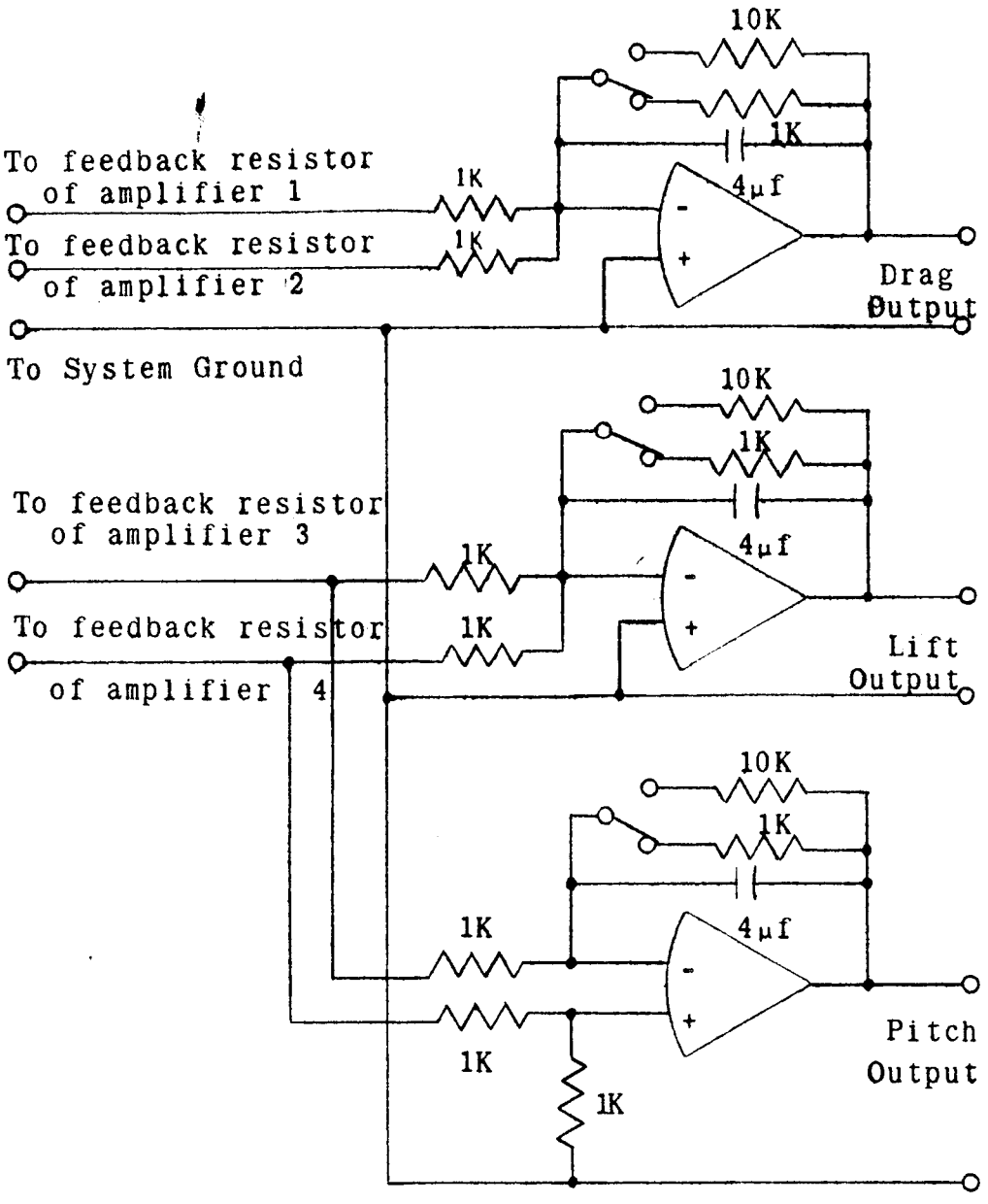

Figure 4-5

Readout Preparation Unit
(Range Switch in 0.05 to 0.5 Position)

CHAPTER V

SYSTEM COMPENSATION

The root locus diagrams that were sketched in Figs. (2-6) and (2-7) show that the system should be stable for any value of gain greater than zero if the assumptions were correct. It was stated in connection with these diagrams, however, that any possible resonances in the mechanical parts of the system had been disregarded and that these factors would probably influence the stability of the system. This was, in fact, the case because when the uncompensated loop was closed the system oscillated.

The frequency of oscillation along both axes was observed, and a rough, trial and error compensation was effected with a somewhat lower value of gain than the desired value. The system had to be made stable in order to take data for a final compensation since even an extremely small force such as a wind current in the room could cause the gas bearing to drift to one of its limits. Once the system was made closed-loop stable, the gas bearing was positioned; and a sinusoidal variable frequency signal could be inserted into the loop. The rough compensation was applied to the forward path of the servo amplifier.

The frequency response data for one y-direction loop was taken as shown in Fig. (5-1). The servo amplifier was not included in the data loop because the frequency response

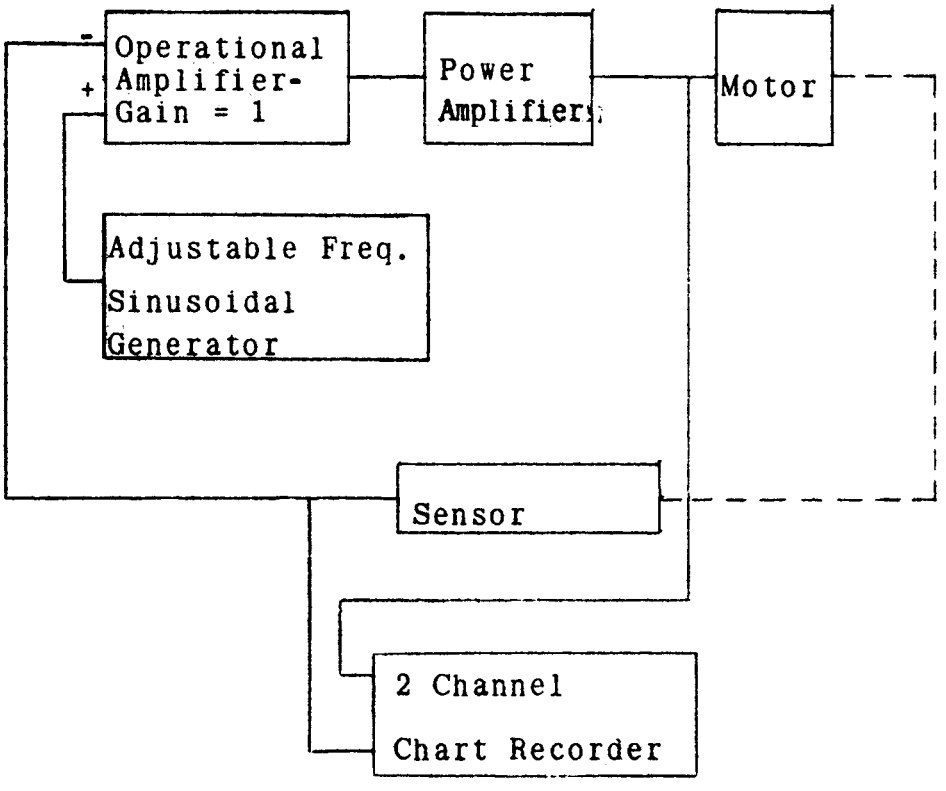

Figure 5-1

Method of Obtaining Open Loop Frequency Response Data

of this component had been altered by the rough compensation, and it was known that the time constants of the amplifier were not significant compared to the time constants of the mechanical part of the system. The gain data that was taken was multiplied by the gain of the servo amplifier and the result plotted as shown in Fig. (5-2).

This graph shows that there are resonances in the mechanical part of the system that were not considered in arriving at the transfer function of Chapter II. This was to be expected because of the long aluminum rod that served as a sting and because of the magnet arm and sensor mounts. No attempt was made to consider analytically the effect of these parts of the system because of the difficult shapes involved and the lack of time imposed by a delivery date for the prototype.

The straight-line approximation of Fig. (5-2) was drawn with the desired gain of 2000 pounds/inch as shown in Fig. (5-3). This straight-line or asymptote approximation was used to determine the asymptote approximation of the compensated system response also shown in Fig. (5-3). Several different attempts were made with the resulting phase margin for each attempt shown. The effect of the sharp upward break at 15 Hz was ignored. It produces a value of phase margin that should be slightly conservative. Because the phase margin values were considered to be conservative, the compensated response with the minimum phase

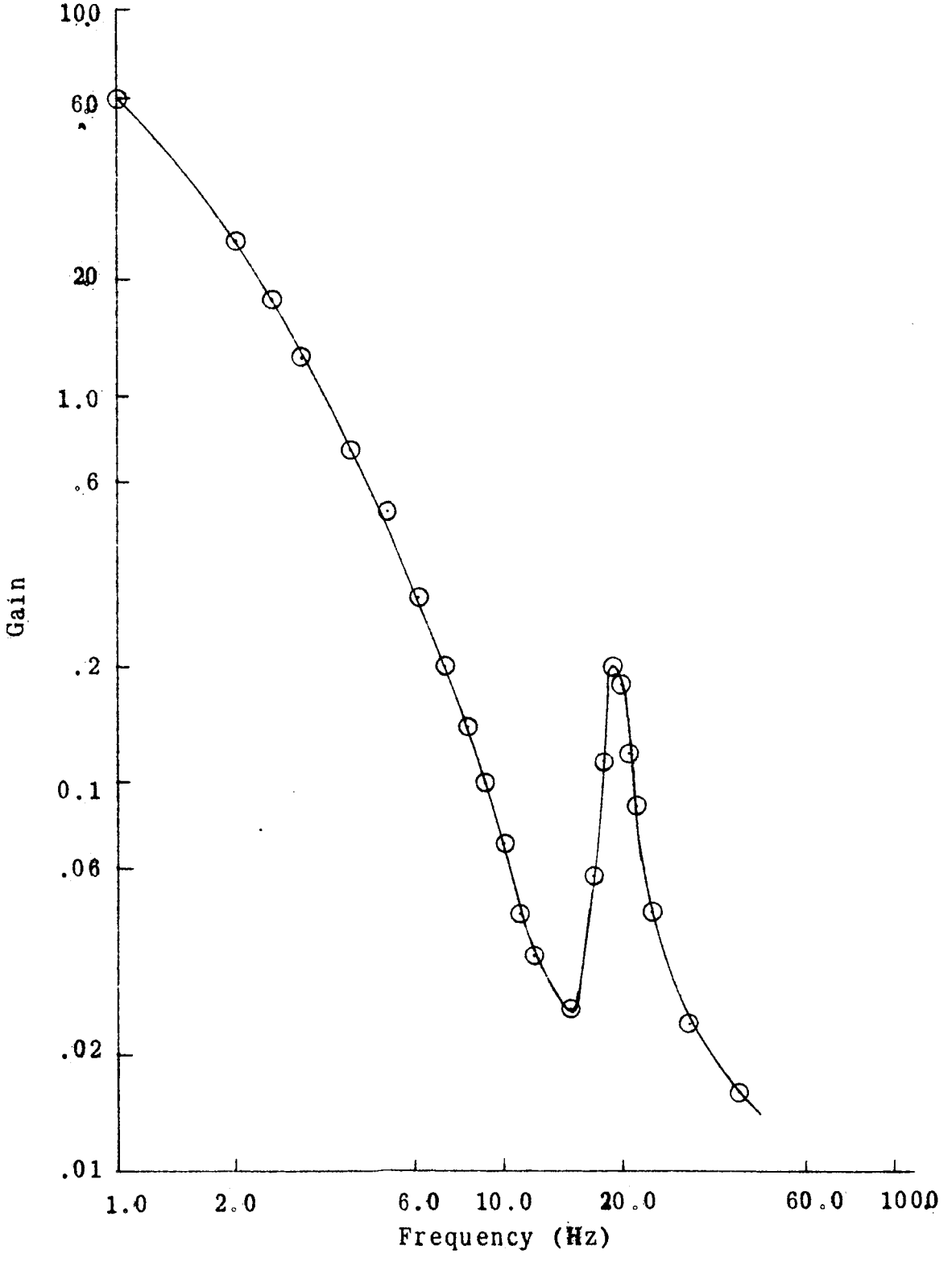

Figure 5-2
Frequency Response of Uncompensated Balance System

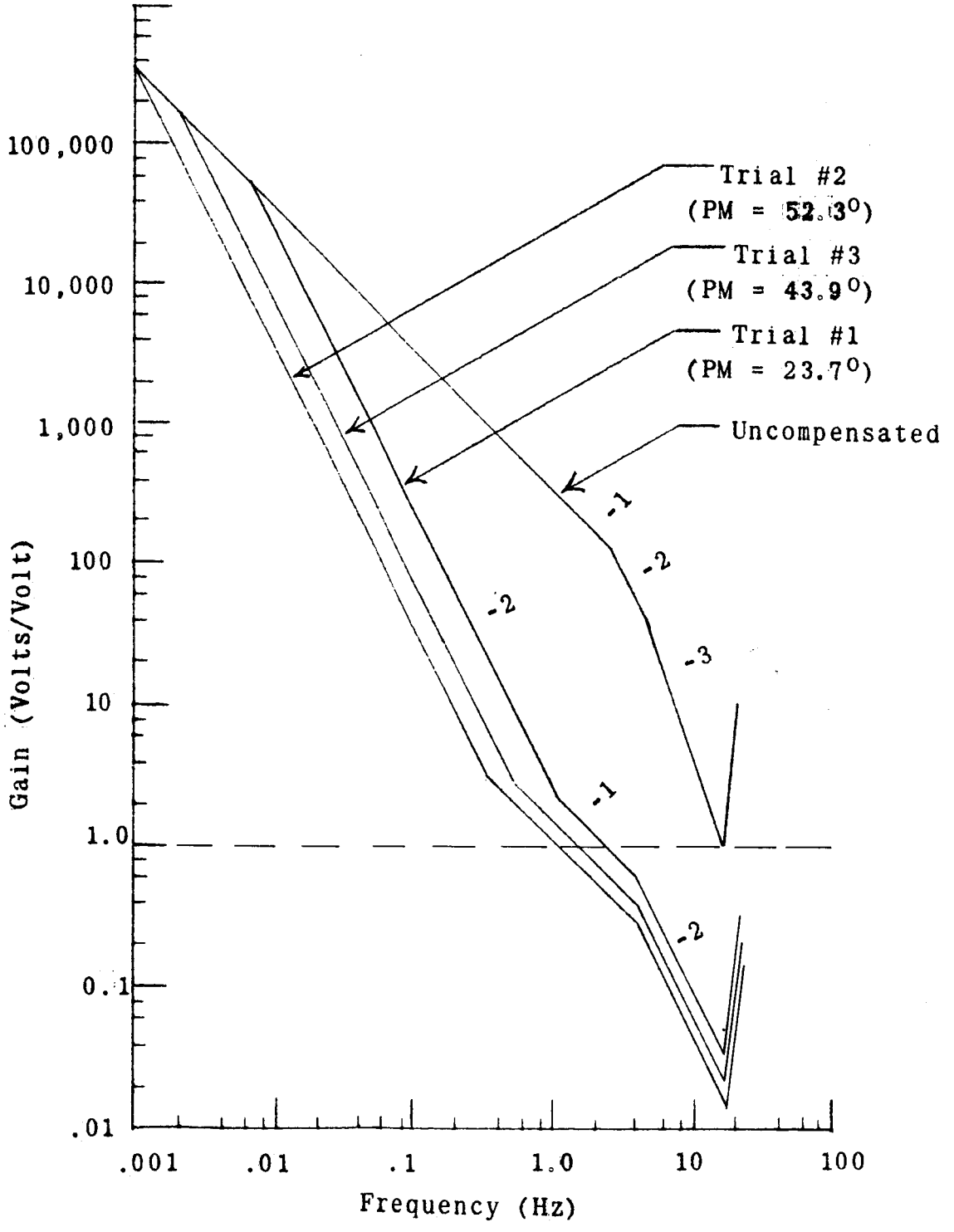

Figure 5-3

Bode Diagram of Y-Direction Servo

margin, 24^{o}, was chosen to determine the necessary compensation. This choice was based on a compromise between relative stability and component size (particularly capacitors) necessary to produce a pole for the lowest break point, 0.006 Hz.

The asymptotic approximation of the compensated response shows that the following response shaping elements are necessary:

1. A pole at 0.006 Hz
2. A zero at 1.2 Hz
3. A zero at 2.6 Hz

It also shows that an additional gain factor of 46 must be included to achieve the desired steady-state displacement.

All of the compensation, including the additional gain, can be obtained with an operational amplifier and R-C networks. The required compensation transfer function can be obtained with the configuration of Fig. (5-4). In this circuit the gain is Z_f/Z_1. The transfer function is

$$\frac{e_o}{e_2} = \frac{R_1R_2C_3}{R_1+R_2} \frac{(s+\frac{1}{R_1C_1})(s+\frac{1}{R_3C_3})}{(s+\frac{1}{(R_1+R_2)C_1})} \qquad (5\text{-}1)$$

The component values are fixed by the time constants given above and by the D. C. gain, keeping in mind that the capacitors should not be polarized and therefore must have relatively low capacitance values. The designer is free to

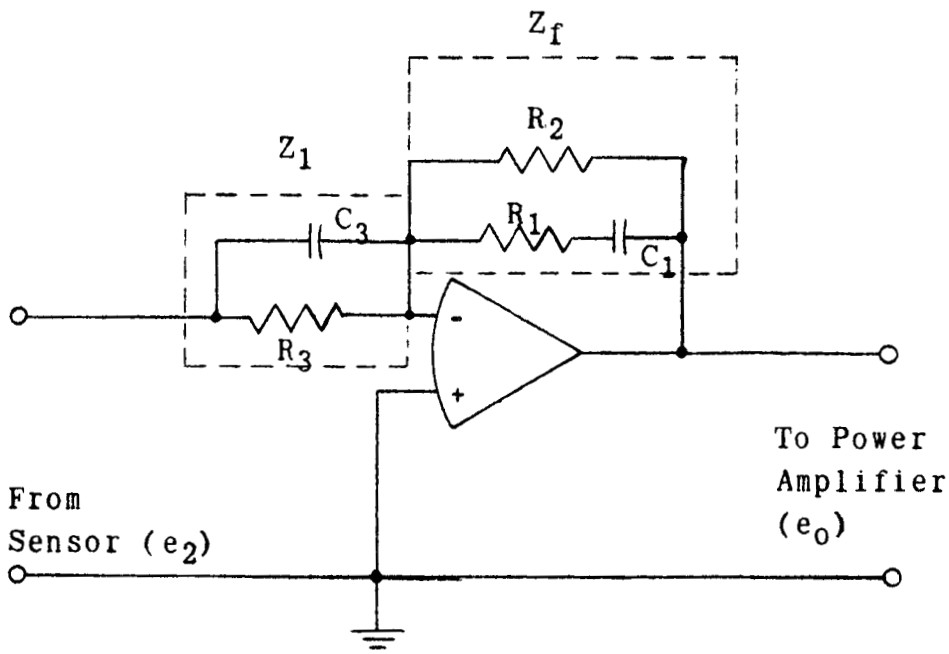

Figure 5-4

Schematic of Compensation Network
For Y-Direction Servo

establish the impedance level. The dc gain is given by:

$$\frac{E_o}{E_2} = \frac{R_2}{R_3} \qquad (5\text{-}2)$$

Because C_1 will be the largest capacitor and because R_1 is determined only by the zero that is to be obtained, this R-C combination will be used to produce the zero at the lower frequency, 1.2 Hz. This leaves R_3 and C_3 to produce the zero at 2.6 Hz.

As a practical maximum, C_1 was chosen to be 12 μf. This determines R_2 because R_1 will be very small compared to R_2. Since R_2 is determined, R_3 is determined by the D. C. gain specification. C_3 is determined by R_3 and the frequency of the zero to be obtained, 2.6 Hz. Thus all the component values can be determined. They are:

R_1 - 10K ohms

R_2 - 2.2M ohms

R_3 - 39K ohms

C_1 - 12 μf

C_3 - 1.5 μf

The circuit of Fig. (5-4) with the component values listed above was inserted into the two y-direction servo loops between the sensor and the power amplifier. The two y-direction servos were stable and the response was considerably faster than the required response of several tenths of a second. The balance system exhibited only one overshoot

before settling.

Due to the lack of time to take data properly on the x-direction servo loop, it was decided that the same compensation would be tried. The component values would have had to be recalculated for this loop because the uncompensated gain for this loop is higher than the uncompensated y-direction loops by a factor of thirteen, but the sensor was provided with an adjustable gain control. Therefore, the gain was lowered by a factor of thirteen by adjusting the gain of the sensor, and the same compensation network was inserted. Because the operational amplifier would have had to drive two power amplifiers, thus exceeding its rating, a current booster amplifier was placed between the operational amplifier and the power amplifier. This compensation also stabilized this loop, and the response was well within specifications; in fact, it was found that the gain could be increased making this servo even stiffer than the y-direction servos.

CHAPTER VI

CONCLUSIONS AND RECOMMENDATIONS

The system has been constructed and is ready to be placed in operation. A second slightly modified model is being built by NASA (Langley) which will be used in a tunnel test facility. Three views of the completed prototype are shown in Figs. (6-1), (6-2) and (6-3).

The performance of this balance system has been described by Mason (4, 5). In essence, Mason found that the system measurements were accurate to within $\pm$ 0.2% of the full scale value for each range, and that the cross-coupling was less than 1% of the full scale value for each range. Thus it can be concluded that the system in its present state of development is suitable for wind tunnel measurements.

Because the theory that is basic to this type of force measurement has now been investigated, further work should center upon improvement of the system. Based upon the previous work, the most fruitful areas for further research appear to be:

1. The causes and effects of cross-coupling should be investigated in detail. In order to facilitate this, the theory of multiple input control systems should be considered as a possible tool.
2. The feasibility of inserting an integration

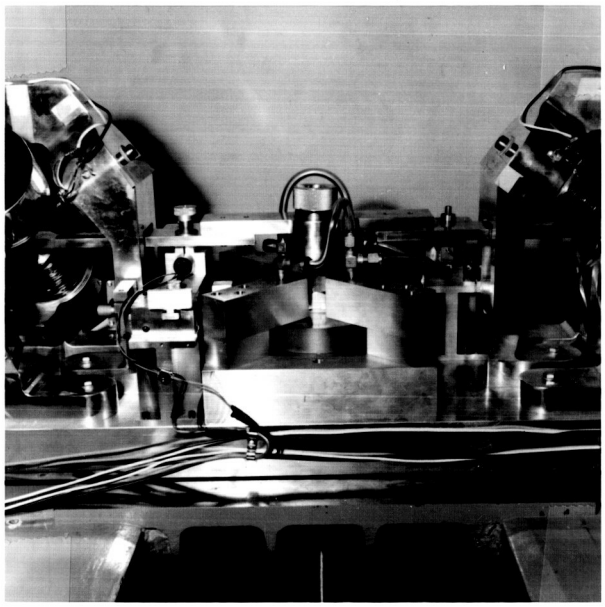

Figure 6-1
Side View of Gas Bearing and Magnet Support
Arm Showing Y-direction Sensors

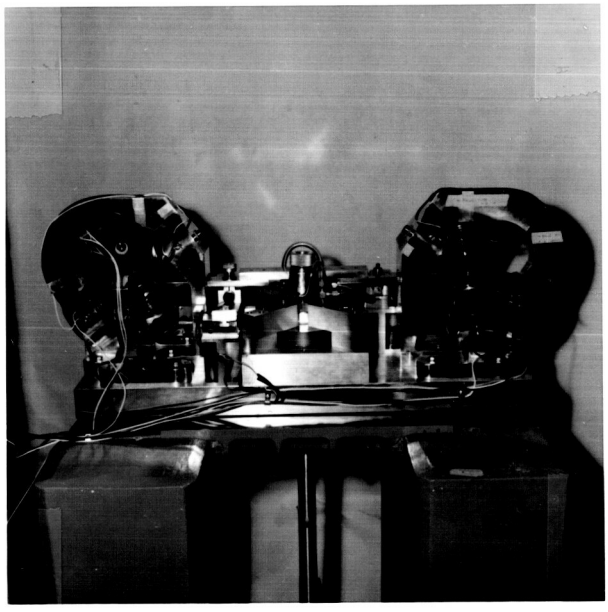

Figure 6-2

Side View Showing Gas Bearing, Motors,
Magnet Support Arm, and Y-direction Sensors

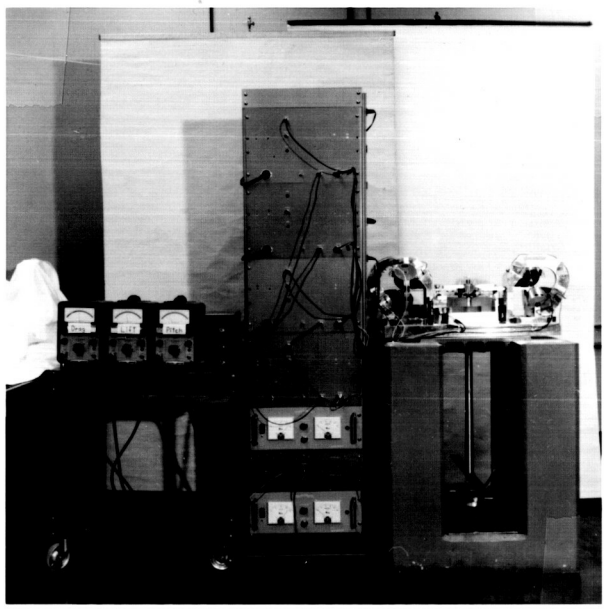

Figure 6-3
Complete Balance System

electronically or mechanically into the feedback path of the sensors should be considered in order to eliminate the steady-state displacement. This is probably one of the principle causes of cross-coupling.

3. A small amplitude, high frequency limit cycle was observed when the system was operated. Time did not permit the close examination of this limit cycle, but it is believed to be due to the resolution of the sensors. The ultimate resolution of the sensor depends upon the dimension of the ferromagnetic domains parallel to the axis of the core. The finite size of these domains probably produces a very narrow width deadband region about the null position. This should be investigated even though the limit cycle was not bothersome due to its small amplitude and relatively high frequency.
4. The accuracy of the system is somewhat limited by noise. This noise has two main sources - system electronics and background vibrations. The noise due to the electronics of the system is considerably less significant, and more easily corrected, than the background vibrations. The sources of background vibrations are sometimes impossible to control, and therefore, the isolation of the system from this source of noise should be investigated.

5. Because the lack of time did not permit the taking of complete frequency response data on the x-direction loop and one of the y-direction loops, this data should be taken and the compensation accordingly changed.

The topics above are just a few of the many possible areas for further study. One very convenient addition to the system would be a provision for auto-calibration. This would eliminate the necessity for manual data reduction.

BIBLIOGRAPHY

(1) Moore, J. W. and E. S. McVey. "A Research Proposal for the Development of Systems and Techniques for Multi-Component Micro-Force Measurements on Wind Tunnel Models", Research Laboratories for the Engineering Sciences, Proposal No. EME-NASA-140-64U (University of Virginia, Charlottesville, September 1964).

(2) Hicks, David A. "Design and Development of a Gas-Supported Hydrostatic Thrust Bearing". M. S. Thesis. Charlottesville, Virginia: University of Virginia, 1965.

(3) Moore, J. W. and E. S. McVey. "Investigation of Systems and Techniques for Multi-Component Micro-Force Measurements on Wind Tunnel Models", Research Laboratories for the Engineering Sciences, Semiannual Status Report No. EME-4029-101-65U (University of Virginia, Charlottesville, August 1965).

(4) Mason, William T., III. "Calibration of a Multi-Component Micro-Force Balance System for Wind Tunnel Models". M. S. Thesis. Charlottesville, Virginia: University of Virginia, 1966.

(5) Moore, J. W., E. S. McVey, and W. T. Mason III. "Calibration of a Multi-Component Micro-Force Balance System for Wind Tunnel Models", Research Laboratories for the Engineering Sciences, Semiannual Status Report No. EME-4029-103A-66U (University of Virginia, Charlottesville, July 1966).

(6) Russell, Robert E. Unpublished memorandum. Charlottesville, Virginia: Research Laboratories for the Engineering Sciences, 1966.

(7) Jenkins, A. W. and H. M. Parker. "Electromagnetic Support Arrangement with Three-Dimensional Control. I. Theoretical", Journal of Applied Physics Supplement, Vol. 30, No. 4, 2385-2395, April 1959. New York: The American Institute of Physics.

(8) Smith, Gregory A. "A Semi-Active Magnetic Support System for Gyroscope Application". M. S. Thesis.

Charlottesville, Virginia: University of Virginia, 1963.

(9) Indiana General Corporation, Magnet Division. "Design and Application of Permanent Magnets", Manual No. 7. Valpariso, Indiana: Indiana General Corporation.

(10) Schaevitz Engineering. "Notes on Linear Variable Differential Transformers", Bulletin AA-1A. Pennsauken, New Jersey: Schaevitz Engineering, 1955.

(11) Schaevitz Engineering. "Standard Linear Variable Transformers", Bulletin AA-2A. Pennsauken, New Jersey: Schaevitz Engineering.

(12) G. L. Collins Corporation. Information provided with product. Long Beach, California: G. L. Collins Corporation.

(13) Schaevitz Engineering. "Corepull Versus Excitation Frequency", Drawing AX-3227. Pennsauken, New Jersey: Schaevitz Engineering, 1960.

(14) Morrison, Charles F., Jr. Generalized Instrumentation for Research and Teaching. Pullman, Washington: Washington State University, 1964.

(15) Stratton, Julius A. Electromagnetic Theory. New York: McGraw-Hill Book Company, Inc., 1941.

(16) Plonsey, Robert and R. E. Collin. Principles and Applications of Electromagnetic Fields. New York: McGraw-Hill Book Company, Inc., 1961.

APPENDIX

DERIVATION OF MOTOR RELATIONS

MOMENT AND GRADIENT COIL CONFIGURATION

As stated in Chapter III, the servo motors that were used in the system were derived from the magnetic support systems. The development given in this appendix follows work by Jenkins and Parker (7) and by Smith (8).

According to Stratton (15) the force on a piece of magnetic material of volume dV located in a magnetic field is given by

$$\overline{dF} = \nabla(\overline{dM} \cdot \overline{B}) \qquad \text{(A-1)}$$

where ∇ is the vector differential operator, $\overline{dM}$ is the incremental magnetic moment of the material, and $\overline{B}$ is the magnetic field.

Equation (A-1) can be expanded to

$$\overline{dF} = (\overline{dM} \cdot \nabla)\overline{B} + (\overline{B} \cdot \nabla)\overline{dM} + \overline{dM}X(\nabla X\overline{B}) + \overline{B}X(\nabla X\overline{dM}) \qquad \text{(A-2)}$$

This equation can be simplified if it is assumed that the moment is an ideal moment, i.e. that the moment originated from a dipole source. In this case the second term on the right in Eq. (A-2) vanishes. If the material is assumed to

be uniformly magnetized, the last term on the right vanishes since $\nabla X \overline{dM} = 0$. The third term on the right vanishes since the volume of the magnetic material encloses no current. Thus, Eq. (A-2) reduces to

$$\overline{dF} = (\overline{dM} \cdot \nabla)\overline{B} \tag{A-3}$$

Because the material has been assumed to be uniformly magnetized, the incremental moment can be expressed as

$$\overline{dM} = \overline{M}dV \tag{A-4}$$

where $\overline{M}$ is the total magnetic moment of the material. Thus, the force equation now becomes

$$\overline{dF} = (\overline{M}dV \cdot \nabla)\overline{B} \tag{A-5}$$

If the moment is oriented as shown in Fig. (A-1), the moment can be expressed as

$$\overline{M} = M_o(\hat{i}_\rho \sin\theta + \hat{i}_z \cos\theta) \tag{A-6}$$

where M_o is the magnitude of the moment. Substitution of this into Eq. (A-5) yields

$$\frac{\overline{dF}}{dV} = M_o \left[\hat{i}_\rho \left(\sin\theta \frac{\partial B_\rho}{\partial \rho} + \cos\theta \frac{\partial B_z}{\partial \rho}\right) + \hat{i}_z \left(\sin\theta \frac{\partial B_\rho}{\partial z} + \cos\theta \frac{\partial B_z}{\partial z}\right) \right] \tag{A-7}$$

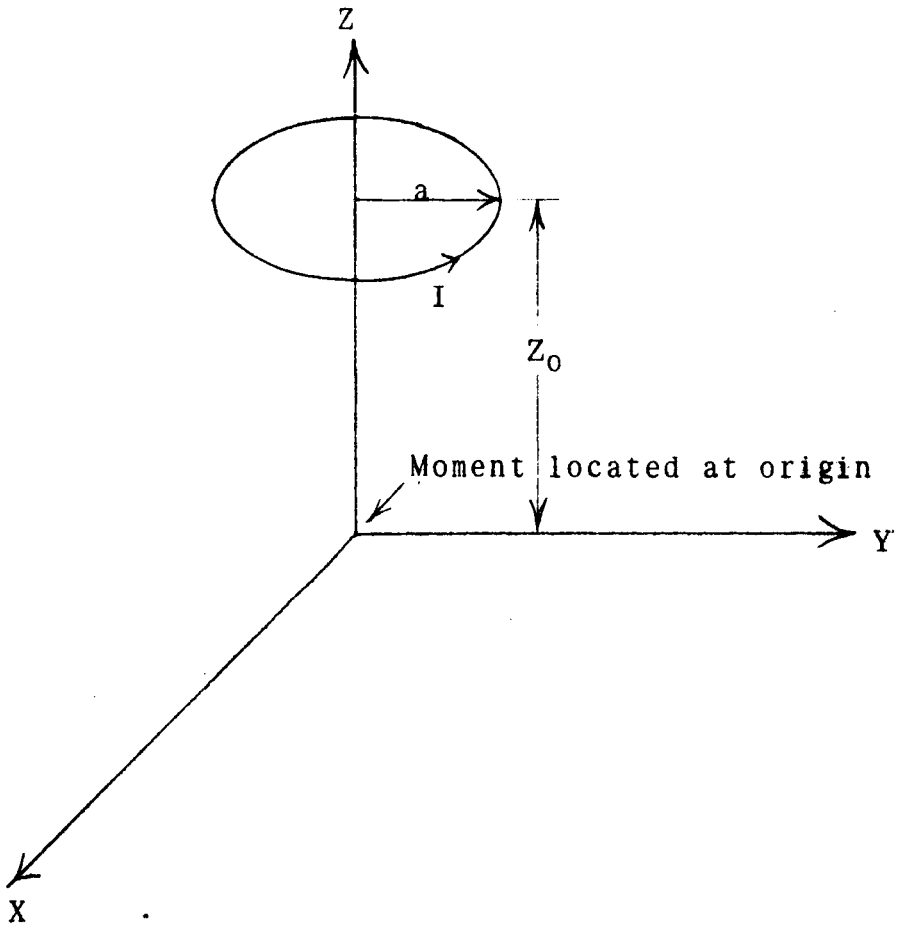

Figure A-1

Geometry for Derivation of Field Due to
Single Circular Loop

since the field, $\bar{B}$, possesses cylindrical symmetry.

Expand B_ρ in a Taylor series for two variables about the origin of the coordinates to obtain:

$$B_\rho(\rho, z) = B_\rho(0, 0) + \rho \left.\frac{\partial B_\rho}{\partial \rho}\right|_o + z \left.\frac{\partial B_\rho}{\partial z}\right|_o + \frac{1}{2!}\left(\rho^2 \left.\frac{\partial^2 B_\rho}{\partial \rho^2}\right|_o + \rho z \left.\frac{\partial^2 B_\rho}{\partial \rho \partial z}\right|_o + z^2 \left.\frac{\partial^2 B_\rho}{\partial z^2}\right|_o\right) + \cdots\cdots \quad \text{(A-8)}$$

Since the motor has two gradient coils that are in series opposition, the field vanishes at the origin. If $\rho \to 0$, the field along the z-axis is obtained. Thus,

$$B_\rho(0, z) = z \left.\frac{\partial B_\rho}{\partial z}\right|_o + z^2 \left.\frac{\partial^2 B_\rho}{\partial z^2}\right|_o + \cdots\cdots \quad \text{(A-9)}$$

The ρ-component of the field vanishes everywhere along the z-axis since it is the axis of symmetry. Therefore,

$$z \left.\frac{\partial B_\rho}{\partial z}\right|_o + z^2 \left.\frac{\partial^2 B_\rho}{\partial z^2}\right|_o + \cdots\cdots = 0 \quad \text{(A-10)}$$

This can be true everywhere along the axis only if the partial derivatives of all orders vanish. A similar development will show that the partials of B_z with respect to ρ also vanish. Thus Eq. (A-7) reduces to

$$\frac{\overline{dF}}{dV} = M_o\left(\hat{i}_\rho \sin\theta \frac{\partial B_\rho}{\partial \rho} + \hat{i}_z \cos\theta \frac{\partial B_z}{\partial z}\right) \quad \text{(A-11)}$$

The total force can be found by integrating Eq. (A-11) over the volume of the permanent magnet, but since the magnet has been replaced by a moment, the total force is

$$\bar{F} = M_o V(\hat{i}_\rho \sin\theta \frac{\partial B_\rho}{\partial \rho} + \hat{i}_z \cos\theta \frac{\partial B_z}{\partial z}) \qquad \text{(A-12)}$$

Throughout this development it has been assumed that the demagnetizing effect of the gradient field on the permanent magnet was negligible.

Now it is necessary to determine what angle, θ, between the moment and the axis of the gradient coils will produce a force that is orthogonal to the moment.

It is known that

$$\nabla \cdot \bar{B} = 0 \qquad \text{(A-13)}$$

since $\bar{B} = \nabla \times \bar{A}$ where $\bar{A}$ is the magnetic vector potential of the field, and $\nabla \cdot \nabla \times \bar{A} = \nabla \cdot \bar{B} = 0$ since the divergence of the curl of a vector is identically zero.

From Eq. (A-13) in cylindrical coordinates, we obtain

$$\nabla \cdot \bar{B} = \frac{1}{\rho} \frac{\partial}{\partial \rho} (\rho B_\rho) + \frac{\partial B_z}{\partial z} = 0 \qquad \text{(A-14)}$$

or

$$\frac{B_\rho}{\rho} + \frac{\partial B_\rho}{\partial \rho} + \frac{\partial B_z}{\partial z} = 0 \qquad \text{(A-15)}$$

In the limit as $\rho \to 0$, $\frac{B_\rho}{\rho} \to \frac{\partial B_\rho}{\partial \rho}$. Therefore

$$\frac{\partial B_\rho}{\partial \rho} = -\frac{1}{2}\frac{\partial B_z}{\partial z} \tag{A-16}$$

at the origin.

Substitution of Eq. (A-16) into Eq. (A-12) gives

$$\bar{F} = M_o V(-\hat{i}_\rho \frac{\sin\theta}{2} \frac{\partial B_z}{\partial z} + \hat{i}_z \cos\theta \frac{\partial B_z}{\partial z}) \tag{A-17}$$

In order for the force and the moment to be orthogonal, the following must hold:

$$\bar{M} \cdot \bar{F} = 0 \tag{A-18}$$

Therefore,

$$\bar{M} \cdot \bar{F} = M_o^2 V \frac{\partial B_z}{\partial z}(-\frac{1}{2}\sin^2\theta + \cos^2\theta) = 0 \tag{A-19}$$

which yields

$$\theta = \tan^{-1}\sqrt{2} \tag{A-20}$$

Therefore, the angle between the axis of the gradient coils and the magnetic moment should be 54.7°.

DESIGN EQUATION

Now that the physical arrangement of the magnet and gradient coils has been determined, it is necessary to try to derive an expression for the force which would be useful for design purposes.

Figure (3-2) shows the physical configuration of the

motor. The magnet is mounted with the long axis vertical giving a vertical moment. The angle between the moment and the gradient coil axis that gives a force perpendicular to the moment has been determined in Eq. (A-20). With this angle, the force is in the xy-plane of the coordinate system of the balance as desired.

The magnitude of Eq. (A-17) is:

$$| \bar{F} | = M_o V \frac{\partial B_z}{\partial z} \sqrt{\frac{\sin^2\theta}{4} + \cos^2\theta} \qquad \text{(A-21)}$$

When the value of angle determined by Eq. (A-20) is substituted into Eq. (A-21), the magnitude of the force in the xy-plane of the balance system is:

$$| \bar{F} | = 0.707\, M_o V \frac{\partial B_z}{\partial z} \qquad \text{(A-22)}$$

Therefore, in order to obtain an explicit expression for the force, the z-component of the field for the particular coil configuration must be determined.

The expression for the field can be obtained by considering the field along the axis due to a single circular loop and then integrating the result over the cross-section of the desired gradient coil shape. The geometry is shown in Fig. (A-1). The field along the axis due to the circular loop is (16):

$$B_z = \frac{\mu_o I}{2} \frac{a^2}{(a^2 + z_o^2)^{3/2}} \qquad \text{(A-23)}$$

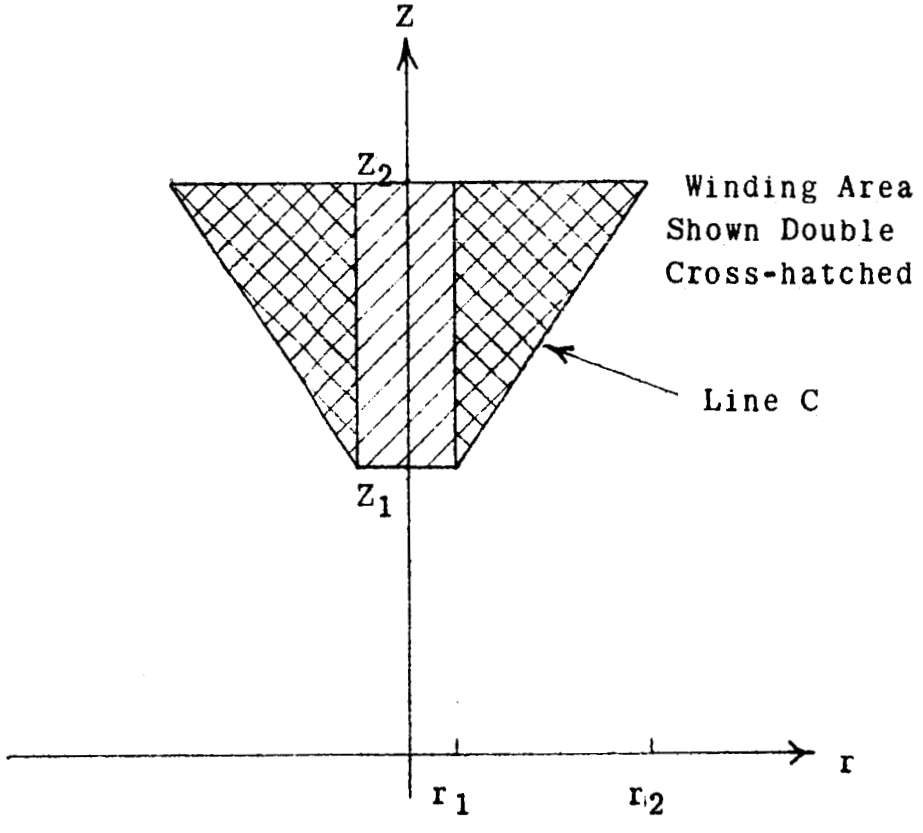

Figure A-2

Schematic of Cross-section of Gradient Coil

where a is the radius of the circular loop, I is the current through the loop, z_o is the distance of the loop from the origin, and μ_o is the permeability of free space.

If this equation is doubled (there are two gradient coils for each motor), and the derivative with respect to the axial coordinate is taken, the following expression results:

$$\frac{\partial B_z}{\partial z_o} = \frac{3\mu_o I a^2 z_o}{(a^2+z_o^2)^{5/2}} \tag{A-24}$$

where the magnet is considered to be midway between the two loops, and the negative sign resulting from the differentiation has been dropped.

The cross-section of a gradient coil is shown in Fig. (A-3), and the integration that must be performed is:

$$\int_A \frac{\partial B_z}{\partial z}\, dA = K \int_A \frac{a^2 z}{(a^2+z^2)^{5/2}}\, dA \tag{A-25}$$

The substitution,

$$K = 3\mu_o J_A \tag{A-26}$$

where J_A is the current density of the coil, has been made in Eq. (A-25).

The general equation of the line C in Fig. (A-3) is:

$$z = mr + b \tag{A-27}$$

where m is the slope and b is the vertical axis intercept. The slope and intercept are given by:

$$m = \frac{z_2 - z_1}{r_2 - r_1}, \quad b = \frac{z_1 r_2 - z_2 r_1}{r_2 - r_1} \tag{A-28}$$

The equation for the force becomes:

$$|F| = K_1 \int_{r_1}^{r_2} r^2 dr \int_{0}^{z=mr+b} \frac{z\,dz}{(r^2+z^2)^{5/2}} \tag{A-29}$$

where

$$K_1 = (0.707\ M_o V)(3\mu_o J_A) \tag{A-30}$$

or

$$K_1 = 2.66 \times 10^{-6} M_o V J_A \tag{A-31}$$

Equation (A-29) can be evaluated by evaluating the second integral first and then integrating the result by parts. The result of this evaluation is the force generated by one servo motor in the xy-plane of the balance system. Thus,

$$|F| = \frac{K_1}{3} \log\left(\frac{r_2}{r_1}\right) - \frac{K_1}{3} \left\{ \frac{1}{4cb^2 - 4m^2b^2} \left[- \frac{4mbr^2 + 4dr}{(cr^2+2mbr+b^2)^{1/2}} \right.\right.$$
$$\left. + 4mb \left(\frac{(cr^2+2mbr+b^2)^{1/2}}{c} \right.\right. \tag{A-32}$$
$$\left.\left. - \frac{mb}{c^{1/2}} \log \left| 2(c^2r^2+2mbcr+cb^2)^{1/2} + 2cr + 2mb \right| \right) \right.$$

$$+ \frac{4b^2}{c^{\frac{1}{2}}} \log \left| 2(c^2r^2+2mbcr+cb)^{\frac{1}{2}} + 2cr + 2mb \right| \Bigg\}_{r_1}^{r_2}$$

where

$$c = 1 + m^2 \tag{A-33}$$

When the values of the parameters were substituted into Eq. (A-32), the resulting force was:

$$|F| = 4.45 \text{ pounds} \tag{A-34}$$

This force is somewhat greater than an order of magnitude in error. Therefore, this design equation should only be used as a very rough check on a design arrived at by the methods of Chapter III or by other, more exact, methods to be developed in the future.

The error in the value given by Eq. (A-32) is probably due to the approximations that were necessary to make the solution tractable to manual methods of computation. This work is presented so that others may use it as a starting point. Obviously, it is of no practical value for motor design in its present form.

ERATUM

FINAL REPORT

on

NASA Grant NGR 47-005-026

Submitted by Co-Principal Investigators:

Dr. James W. Moore

Dr. Eugene S. McVey

and

Karl C. Henderson

Research Laboratories for the Engineering Sciences

University of Virginia

Charlottesville

Report No. EME-4029-103C-66U

August 1966

CHAPTER I

INTRODUCTION

GENERAL

A system is described in this report which is used to measure forces on wind tunnel models. The primary emphasis of the report is on the electronic design and operation of the system because other reports describe the air bearing design (Report No. EME-4029-101-65U issued August 1965) and calibration (Report No. EME-4029-103A-66U issued July 1966). Although the system was developed to make force measurements on wind tunnel models, it is believed that the basic ideas developed can be used on other force measurement problems, e.g., ion engine thrust measurements.

Analytical and experimental work through the prototype stage has been completed, and actual wind tunnel operation should take place soon. The prototype is an operational system that can be effectively used in wind tunnels to measure nominal, axial and pitch force magnitudes from 0.005 pound to 0.5 pound in two ranges.

This work was necessitated by requirements to measure relatively small multi-component forces to an accuracy of 1% or better. Minimization of cross coupling was a design goal. The problem was complicated by the ratio of model weight to aerodynamic force on the model. A typical range for this ratio is 100:1 to 1:1. These ratios are a result of the necessity to use relatively small heavy models for hypersonic velocity studies. The models are heavy because they must be made of heat resistant materials and the size is affected by the practical need to make hypersonic tunnel dimensions small.

CHAPTER VI

CONCLUSIONS AND RECOMMENDATIONS

An engineering development model has been constructed and will be placed in operation soon. This model was originally built to establish system feasibility and was intended to serve as a guide for the construction of another model for actual tunnel measurements. However, sufficient time is not available to build the second model before tunnel testing starts. Three views of the completed prototype are shown in Figs. (6-1), (6-2) and (6-3).

The performance of this balance system has been described by Mason (4, 5). In essence, Mason found that the system measurements were accurate to within ± 0.2% of the full scale value for each range, and that the cross-coupling was less than 1% of the full scale value for each range. Thus, it can be concluded that the system in its present state of development is suitable for wind tunnel measurements.

Because the theory that is basic to this type of force measurement has now been investigated, further work should center upon improvement of the system. Based upon the previous work, the most fruitful areas for further research appear to be:

1. The causes and effects of cross-coupling should be investigated in detail. In order to facilitate this, the theory of multiple input control systems should be considered as a possible tool.
2. The feasibility of inserting an integration.